



# Perinatal interference with the serotonergic system affects VTA function in the adult via glutamate co-transmission

Catarina Cunha<sup>1,2</sup> · John F. Smiley<sup>1,2</sup> · Nao Chuhma<sup>3,4</sup> · Relish Shah<sup>1</sup> · Cynthia Bleiwas<sup>1</sup> · Edenia C. Menezes<sup>1</sup> · Rebecca P. Seal<sup>5</sup> · Robert H. Edwards<sup>6</sup> · Stephen Rayport<sup>3,4</sup> · Mark S. Ansorge<sup>3,7</sup> · Francisco X. Castellanos<sup>1,2</sup> · Catia M. Teixeira<sup>1,2</sup>

Received: 14 May 2019 / Revised: 7 April 2020 / Accepted: 27 April 2020 / Published online: 12 May 2020  
© The Author(s), under exclusive licence to Springer Nature Limited 2020

## Abstract

Serotonin and dopamine are associated with multiple psychiatric disorders. How they interact during development to affect subsequent behavior remains unknown. Knockout of the serotonin transporter or postnatal blockade with selective serotonin reuptake inhibitors (SSRIs) leads to novelty-induced exploration deficits in adulthood, potentially involving the dopamine system. Here, we show in the mouse that raphe nucleus serotonin neurons activate ventral tegmental area dopamine neurons via glutamate co-transmission and that this co-transmission is reduced in animals exposed postnatally to SSRIs. Blocking serotonin neuron glutamate co-transmission mimics this SSRI-induced hypolocomotion, while optogenetic activation of dopamine neurons reverses this hypolocomotor phenotype. Our data demonstrate that serotonin neurons modulate dopamine neuron activity via glutamate co-transmission and that this pathway is developmentally malleable, with high serotonin levels during early life reducing co-transmission, revealing the basis for the reduced novelty-induced exploration in adulthood due to postnatal SSRI exposure.

**Supplementary information** The online version of this article (<https://doi.org/10.1038/s41380-020-0763-z>) contains supplementary material, which is available to authorized users.

✉ Catia M. Teixeira  
catia.teixeira@nki.rfmh.org

- <sup>1</sup> Emotional Brain Institute, Nathan Kline Institute for Psychiatric Research, Orangeburg, NY 10962, USA
- <sup>2</sup> Department of Child and Adolescent Psychiatry, New York University Grossman School of Medicine, New York, NY 10016, USA
- <sup>3</sup> Department of Psychiatry, Columbia University and New York State Psychiatric Institute, New York, NY 10032, USA
- <sup>4</sup> Department of Molecular Therapeutics, New York State Psychiatric Institute, New York, NY 10032, USA
- <sup>5</sup> Department of Neurobiology and Department of Otolaryngology, University of Pittsburgh School of Medicine, Pittsburgh, PA 15260, USA
- <sup>6</sup> Departments of Neurology and Physiology, University of California, San Francisco School of Medicine, San Francisco, CA 94143, USA
- <sup>7</sup> Department of Developmental Neuroscience, New York State Psychiatric Institute, New York, NY 10032, USA

## Introduction

Serotonergic neurons located in the dorsal and medial raphe nuclei (RN) project throughout the brain, modulate a wide range of neuronal processes, and are critical in the development of brain circuits [1]. Alterations in serotonergic activity have been associated with several psychiatric disorders and selective serotonin reuptake inhibitors (SSRIs) are key to their treatment [2]. Given the role of serotonin (5HT) in brain development, changes in serotonergic levels during early life may be deleterious for brain and behavioral development [3]. Early life exposure to SSRIs in rodents leads to enduring deficits in adult emotional regulation [4, 5]. Furthermore, studies have implicated gestational exposure to SSRIs in the development of psychiatric disorders in humans [6, 7]. However, the mechanisms by which early life SSRI exposure lead to behavior deficits in adulthood are unknown.

Recent work has uncovered a strong disynaptic pathway linking the dorsal raphe (DR) and the nucleus accumbens (NAc) via the ventral tegmental area (VTA) (DR→VTA→NAc) [8]. Dopaminergic (DAergic) neurons in the VTA have critical roles in reward seeking, motivation, social interaction, and arousal [9, 10]; dopamine (DA) release in the NAc is

linked to behavioral activation and energy expenditure [10]. These observations support the hypothesis that reduced behavioral activation caused by constitutive serotonin-transporter gene ablation (SERT-KO) [11] and perinatal SSRI exposure [4] involve functional changes in the DR > VTA > NAc pathway. While 5HT itself exerts inhibitory effects on DAergic neurons [12–14], it has recently been shown that serotonergic neurons may excite VTA-DAergic neurons via glutamatergic co-transmission [15, 16]. However, these results have been challenged by work that suggest that glutamatergic activation of VTA-DAergic neurons arises from RN non-serotonergic neurons and that activation of serotonergic terminals in the VTA is not rewarding [17, 18].

Here we show that RN serotonergic axons in the VTA co-express vesicular glutamate transporter (VGLUT3), and that optogenetic activation of serotonergic terminals in the VTA can activate DAergic neurons through AMPA receptors. Supporting our hypothesis that the functional properties of the DR > VTA > NAc pathway are sensitive to developmental 5HT perturbation, we show that early postnatal SSRI exposure alters the glutamatergic component of RN to VTA synaptic transmission. Furthermore, we show that exploration deficits observed in mice postnatally exposed to a SSRIs are mimicked by knocking-out VGLUT3 from serotonergic neurons and can be reversed by optogenetic activation of VTA-DAergic neurons.

## Methods

### Subjects

Experiments were performed at the Nathan Kline Institute (NKI) and at the Rodent Neurobehavioral Analysis Core at NYS Psychiatric Institute, Columbia University Medical Center. Experiments were conducted blind to the treatment group and in compliance with the Principles of Laboratory Animal Care National Institutes of Health (NIH) guidelines, under protocols approved by NKI, Columbia University and NYSPI IACUCs. Double transgenics and their single transgenic littermate controls were housed in groups (two to five mice per cage) and maintained on a 12 h light/dark cycle with access to food and water ad libitum. Approximately equal numbers of male and female mice were used in the experiments. Mice were tested as adults, between 3 and 5 months of age. The ePet1-cre [19] line was originally generated on the (C57BL/6 × SJL)F2 background. This line was backcrossed to 129SvEv/Tac for >10 generations. Another set of animals from this line was backcrossed onto a C57BL/6J background for five generations. For conditional expression of channel rhodopsin2 (ChR2), we used the ROSA26-floxed-STOP-CAG-ChR2-EYFP (ChR2<sup>fl/fl</sup>) Ai32 line [20]. This line was generated on the (129S6/SvEvTac × C57BL/6Ncr1)F1

background and was backcrossed to 129SvEv/Tac for 6 generations. Serotonergic neurons express vesicular glutamate transporter expressed VGLUT3 [21].

To ablate VGLUT3 conditionally, we used mice with the conditional *vglut3* allele (VGLUT3<sup>fl/fl</sup>) which were originally derived from 129/Ola ES cells and C57BL/6J blastocysts [22]. Founders were backcrossed 5 generations to C57BL/6J. Floxed mice were crossed with Cre-lines of the same strain. For ChR2 expression in serotonergic terminals, we used Pet1<sup>Cre/+</sup>;ChR2<sup>fl/fl</sup> (Pet1-ChR2) and Pet1<sup>+/+</sup>;ChR2<sup>fl/fl</sup> as controls. For ChR2 expression in serotonergic cell bodies in the RN, mice heterozygous for ChR2 were used: Pet1<sup>Cre/+</sup>;ChR2<sup>fl/fl</sup> (Pet1-ChR2) and Pet1<sup>+/+</sup>;ChR2<sup>fl/fl</sup> (Control). For ablation of VGLUT3 from serotonergic neurons, we used Pet1<sup>Cre/+</sup>;VGLUT3<sup>fl/fl</sup> (VGLUT3-cKO) and Pet1<sup>+/+</sup>;VGLUT3<sup>fl/fl</sup> (Control). To express ChR2 in DAergic neurons selectively we crossed a DA-transporter Cre-driver-line (Dat<sup>IRRES-Cre</sup>) [23] with the ChR2<sup>fl/fl</sup> line. Two genotypes were used: Dat<sup>IRRES-Cre/+</sup>;ChR2<sup>fl/fl</sup> (Dat-ChR2) and Dat<sup>+/+</sup>;ChR2<sup>fl/fl</sup> (Control). We previously showed that hemizygous expression of Pet1<sup>Cre</sup> [24] or Dat<sup>IRRES-Cre</sup> [25] does not produce a behavioral phenotype in the tests used here. The use of conditional ChR2-expressing mice instead of viral vectors produces more consistent labeling of the entire population of cells enhancing between-group comparisons.

### Drugs

Postnatal SSRI treatment: Postnatal day (P)2 pups were randomly assigned to saline (vehicle) or 10 mg/kg fluoxetine treatment groups. The mice received daily i.p. injections of the assigned treatment from P2 to P11 as previously described [5]. For electrophysiology, pharmacological agents were applied to the slice preparation by dissolving them in perfused artificial cerebrospinal fluid (ACSF). CNQX (Sigma) was bath applied in ACSF for 10 min.

### Immunohistochemistry and stereological cell counts

Mice were transcardially perfused with ice cold 0.1 M phosphate-buffered saline followed by buffered 4% paraformaldehyde (PFA). Isolated brains were immersed in PFA overnight and then embedded in agar for simultaneous processing, coronally sectioned into 50 μm thick sections on a freezing microtome and processed for immunofluorescence as previously described [26]. Double or triple immunofluorescent labeling combined primary antibodies from different species, including rabbit anti-5HT (Sigma, Cat# S5545), guinea pig anti-VGLUT3 (Synaptic Systems, Cat# 135204), rabbit anti-tyrosine hydroxylase (TH) (Pel-Freez, Cat# P40101) or mouse anti-TH (Chemicon, Cat# MAB318), and chicken anti-GFP to label ChR2-eYFP expression in Pet1+ neurons (Abcam, Cat# ab13970). For

5HT/VGLUT3 colocalization and RN cells, anti-5HT was visualized with Alexa Fluor 488 secondary antibody (Invitrogen cat# A11034) colocalized with anti-VGLUT3 coupled to a biotinylated antibody (Vectastain Cat# BA-7000) and streptavidin 594 (Invitrogen Cat# S11227). For 5HT/VGLUT3 colocalization in VTA axons, DA cells were additionally visualized with mouse anti-TH and Alexa Fluor 405 goat anti-mouse (Invitrogen Cat# A31553). For PET1/5HT in RN cells, anti-GFP (for PET1 neurons) was coupled to Alexa Fluor 488 antibody (Abcam, cat# 150185) and anti-5HT was coupled to a biotinylated antibody (Vectastain Cat# BA-1000) followed by streptavidin 594. For PET1/VGLUT3 in the RN, anti-GFP coupled to Alexa Fluor 488 was colocalized with anti-VGLUT3 coupled to a biotinylated antibody (Vectastain Cat# BA-7000) followed by streptavidin 594. For PET1/VGLUT3 in the VTA, streptavidin 647 (Invitrogen Cat# S21374) was used to visualize VGLUT3, and TH cells were identified by rabbit anti-TH conjugated to goat anti-rabbit Alexa Fluor 555 (Invitrogen, or A21428).

Stereological estimates of cell number used the fractionator method [27], as previously described [26]. Cell counts in the RN evaluated all 5HT or Pet1 neurons in the cell groups B5 to B9 [28, 29], thus including the dorsal and medial RN and rostrally the suprallemniscal (B9) and caudal linear nuclei. The RN was sampled in every fourth consecutive section, yielding 6–11 sections for analysis. Sections were systematically sampled at a grid of sites, and a Z-stack of six 2  $\mu$ m spaced images was captured at each site with a Foculus FO442 digital camera (Net GMBH, Germany) using a 40 $\times$ , 1.3 numerical aperture (NA) oil-immersion objective. Cell counting was done on optical dissector counting boxes drawn onto each Z-stack. Estimates of measurement precision [30] showed coefficients of error less than 0.1 for all cell number estimates except for the small populations of 5HT+/VGLUT3+ neurons in VGLUT3-KO animals, or the 5HT neurons that lacked Chr2-eYFP.

The frequency of VGLUT3 expression in 5HT axon boutons was estimated in the VTA at or caudal to the level of the medial lemniscus. Axons were sampled using a 63 $\times$  oil objective on a Zeiss 510 confocal microscope, capturing 10–15 z-stack images distributed across the VTA in 2 sections per animal. Each z-stack image had X and Y dimensions of 143  $\mu$ m and 4 equally spaced 1  $\mu$ m optical slices. Colocalization was evaluated by identifying 10 5HT axon boutons per image, that were subsequently evaluated for the presence or absence of VGLUT3 immunofluorescence. The same approach was used to quantify Pet1/VGLUT3 co-expression in fluoxetine experiments, although sampling was restricted to the caudal linear nucleus of the VTA in order to compare with the site of electrophysiological sampling.

The same confocal images through the caudal linear nucleus of the VTA were additionally used to evaluate Pet1 axon density, by counting axon contacts with 16 hemispheric probes evenly distributed across each confocal image [31]. Axon densities are expressed as number of contacts per 4  $\mu$ m diameter hemispheric probe.

### Stereotaxic surgery

Fiber optic implants were prepared using 1.25 mm zirconia ferrules (Precision Fiber Products) with a 200  $\mu$ m optical fiber (ThorLabs) as previously described [32]. Starting at 2 months of age, using standard stereotaxic procedures [33], fiber optic implants were placed targeting the DR (AP:  $-5.0$ , L:  $0$ , DV:  $-3.2$ ), VTA (AP:  $-3.4$ , L:  $+0.5$ , DV:  $-4.3$ ), NAc (AP:  $1.2$ , L:  $\pm 1.4$ , DV:  $-4$ ), PFC (AP:  $1.5$ , L:  $0$ , DV:  $-1.6$ ), or Amygdala (AP:  $-1.1$ , L:  $\pm 3.2$ , DV:  $-4.4$ ). All coordinates are in reference to Bregma. Mice were allowed to recover for at least 2 weeks after surgery.

For labeling of DAergic neurons for electrophysiological recordings we used AAV-TH-dsRed virus. The TH-dsRed plasmid was generously provided by Dr Kwang-Soo Kim's laboratory [34]. AAV-TH-dsRed virus microinjection was performed using a stereotaxically placed glass micropipette. The micropipette was connected via PE tubing to a Hamilton syringe placed in an infusion pump. In total, 200  $\mu$ l deposits of virus were pressure-injected over 5 min. After the injection, the micropipette was left in place for an additional 15 min and then withdrawn slowly. One week was allowed for recovery post-surgery.

### Electrophysiological recording and analysis of DA neuron response to serotonergic terminal stimulation in naïve mice

One week post virus injection, mice (P60–70) were anesthetized with an i.p. injection of ketamine (80 mg/kg)/xylazine (20 mg/kg) mixture. After confirmation of full anesthesia with gentle paw pressure, mice were decapitated and brains removed in ice-cold high-glucose ACSF (in mM: 75 NaCl, 2.5 KCl, 26 NaHCO<sub>3</sub>, 1.25 NaH<sub>2</sub>PO<sub>4</sub>, 0.7 CaCl<sub>2</sub>, 2 MgCl<sub>2</sub> and 100 glucose, pH 7.4; saturated with mixture of 95%O<sub>2</sub>–5%CO<sub>2</sub>). In total, 300  $\mu$ m thick horizontal sections of the ventral midbrain were made with a vibratome (VT1200S, Leica). The slices were preincubated in high-glucose ACSF for 1 h at room temperature for recovery, then transferred to the recording chamber (submerged, 500  $\mu$ l volume) on the stage of an upright fluorescent microscope (BX61WI, Olympus), which was continuously perfused with regular ACSF (in mM: 125 NaCl, 2.5 KCl, 25 NaHCO<sub>3</sub>, 1.25 NaH<sub>2</sub>PO<sub>4</sub>, 2 CaCl<sub>2</sub>, 1 MgCl<sub>2</sub> and 25 glucose, pH 7.4; saturated with mixture of 95%O<sub>2</sub>–5%CO<sub>2</sub>).

Recorded neurons were visualized using enhanced visible light differential interference contrast (DIC) optics with a scientific c-MOS camera (ORCA-Flash4.0LT, Hamamatsu Photonics).

Current clamp and voltage clamp recordings were done at 32–33 °C (TC 344B Temperature Controller, Warner Instruments). DAergic neurons in the lateral VTA and substantia nigra (SN) pars compacta (SNc) were identified visually and confirmed by membrane properties. These DAergic neurons have large oval (lateral VTA) or spindle (SNc) shaped cell bodies, voltage sag at hyperpolarized membrane potentials, relatively slow spontaneous firing (~1–4 Hz), and a slower afterhyperpolarization. For identification of medial VTA-DAergic neurons, which do not show typical DAergic neuron hallmarks, TH-dsRed expression was confirmed by fluorescence stimulated by 590 nm LED illumination (DC4100, Thorlabs). Recording patch pipettes were fabricated from standard-wall borosilicate glass capillary with filament (World Precision Instruments). Pipette resistance was 4–6 M $\Omega$ . Composition of intracellular solution was (in mM): 135 K<sup>+</sup>-methane sulfonate (MeSO<sub>4</sub>), 5 KCl, 2 MgCl<sub>2</sub>, 0.1 CaCl<sub>2</sub>, 10 HEPES, 1 EGTA, 2 ATP and 0.1 GTP, pH 7.25. Some EPSC recordings were performed with Cs<sup>+</sup>-based intracellular solution; K<sup>+</sup>-MeSO<sub>4</sub> was replaced with Cs<sup>+</sup>-MeSO<sub>4</sub>, and QX314 (lidocaine N-ethyl bromide) 5 mM was added to block unclamped Na<sup>+</sup> currents. Recordings from spontaneously active DA neurons were performed with an Axopatch 200B amplifier (Molecular Devices) in fast current-clamp mode or voltage clamp, holding at –70 mV, or +40 mV for NMDA receptor responses. Series resistance (10–30 M $\Omega$ ) was compensated online by 70%. Liquid junction potentials (10–12 mV) were adjusted online. Synaptic responses were evoked with 5 ms field illumination with a high-power blue LED (470 nm; Thorlabs) delivered as a single pulse at 0.1 Hz, or in a train of five pulses at 20 Hz, repeated at 30 s intervals. Drugs were delivered by perfusion.

Electrophysiological signals were filtered at 5 kHz using a 4-pole Bessel filter, digitized at 5 kHz (Digidata 1550A, Molecular Devices) and recorded using pClamp 10 (Molecular Devices). Data were analyzed with Axograph X (Axograph Scientific) and Igor Pro (Wavemetrics). Action potentials were automatically detected with voltage threshold of 0 mV. Baseline firing frequencies were calculated from 2 s windows before train stimulation. Firing z-score during train photostimulation was calculated as the difference of average firing frequency during (0–0.4 s from train onset) and the average baseline firing frequency, divided by the standard deviation of baseline firing frequency. A plus score indicates increased firing from baseline, while a minus score indicates decreased firing. Z-scores larger than +2 or smaller than –2 were regarded as significant increases or decreases of firing, respectively. Amplitudes of evoked EPSCs were evaluated from averages made from 10 consecutive traces. Statistical analyses were done with R 3.5.2

with stats package, or JASP 0.9 (JASP Team, 2019; [www.http://jasp-stats.org](http://jasp-stats.org)). Data are shown as mean  $\pm$  SEM.

### Electrophysiological recording and analysis of DA neuron response to serotonergic terminal stimulation in postnatally treated animals

Mice were anesthetized with a mixture of ketamine (50 mg/kg) and xylazine (4.5 mg/kg) and perfused transcardially with 5–10 ml ice-cold ACSF containing (in mM): 124 NaCl, 3 KCl, 1 CaCl<sub>2</sub>, 1.5 MgCl<sub>2</sub>, 26 NaHCO<sub>3</sub>, 1 NaH<sub>2</sub>PO<sub>4</sub>, and 16.66 glucose, continuously saturated with carbogen (95%O<sub>2</sub> and 5%CO<sub>2</sub>). Horizontal slices of ventral midbrain were transferred to a preincubation chamber with ACSF containing (in mM) 2 CaCl<sub>2</sub>, 1 MgCl<sub>2</sub>, at 35 °C for 60 min, then they were stored at room temperature until recording. The recording electrode contained (in mM) for current-clamp recording: 135 K-gluconate, 7 KCl, 10 HEPES, 10 Na-phosphocreatine, 4 Mg<sub>2</sub>-ATP, and 0.4 NaGTP (290–295 mOsm, pH 7.35 with KOH). Voltage clamp recordings were done with Cs<sup>+</sup>-based pipette solution, which was composed of (in mM): 135 Cs-gluconate, 10 HEPES, 10 Naphosphocreatine, 4 Mg<sub>2</sub>-ATP, and 0.4 NaGTP (290–295 mOsm, pH 7.35 with CsOH). Chr2+ serotonergic terminals in the VTA were stimulated with light pulses (470 nm, 1 ms duration, coherent). Paired-pulse (100 ms interval, between the first and second stimuli) excitatory postsynaptic currents (EPSCs) were recorded from neurons in the VTA. The paired-pulse ratio of the amplitudes (PPR = EPSC2/EPSC1) were calculated from averaged traces made from 3 consecutive traces.

To evaluate AMPA/NMDA ratios, photo-evoked EPSCs of serotonergic neurons onto VTA neurons were recorded at –70 mV and +40 mV. AMPAR currents were measured as peak amplitudes at –70 mV, since NMDAR currents are not observed at that potential because of Mg<sub>2</sub>+block. NMDAR currents were measured at +40 mV at the time point where the AMPAR-current dropped by more than 75% from peak amplitude to minimize AMPAR contribution [35, 36].

### Behavioral testing

After recovery from surgery, mice were tested in the open-field or in the real-time or conditioned place-preference tests. Chr2 and their respective controls were stimulated using blue light pulses (473 nm, 20 Hz, 10 ms, 10 mW). Real-time place preference was performed in a standard rat cage divided into two sections by Plexiglas dividers. During the duration of the test, one side of the cage was paired with optic stimulation (473 nm, 20 Hz, 10 ms, 10 mW) of DR while the other was not (counterbalanced). There were no distinct marks in each side of the cage. In the conditioned-

place-preference test, mice were free to explore a two-sided box for 20 min a day for 2 days. Each side of the box had distinct visual and tactile cues. One side of the chamber was paired with optical stimulation (473 nm, 20 Hz, 10 ms, 10 mW) of the DR (counterbalanced). On the third day the mice were allowed to explore the box for 20 min without stimulation.

We used two apparatus to measure activity. One open field apparatus consisted of square Plexiglas activity chambers equipped with infrared detectors to track animal movement. The other open field apparatus consisted of square Plexiglas activity chambers equipped with video cameras via which the animals were tracked with Anymaze software. Mice were allowed to walk freely over the duration of the trial. Photostimulation (473 nm, 10 mW) was delivered in periods of 180 s (20 Hz, 10 ms pulses). Elevated-Plus Maze, Forced Swim Test, Novelty Suppressed Feeding and Light-Dark preference tests were performed as described [37, 38].

## Statistics

Sample sizes were chosen based on previous studies [5, 25]. Parametric statistical tests were used, with  $\alpha = 0.05$ , two-tailed. Samples presented normal distribution. Student's *t* test was used for comparisons between two groups, and repeated measures ANOVA was used for comparisons between groups across time, followed by *t*-tests correcting for multiple comparisons using the Holm–Sidak method in Prism (GraphPad). Data are expressed as mean  $\pm$  SEM.

## Results

### Serotonergic neurons projecting to the VTA co-express glutamatergic markers

In the raphe, both VGLUT2 and VGLUT3 are present. VGLUT2 is expressed by non-5HT cells while VGLUT3 is expressed in non-5HT neurons and some but not all 5HT neurons [16, 21, 39, 40]. Here, we first characterized the expression of VGLUT3 in 5HT+ neurons of the DR and MR. Plotting the distribution of 5HT+/VGLUT3+ neurons in the RN revealed their presence throughout the rostral-caudal extent of the DR, with high density in the ventral subdivision (DRv) and few 5HT+/VGLUT3+ neurons in the dorsal (DRd) and lateral (DRl) subdivisions (Fig. 1a). In addition, 5HT+/VGLUT3+ neurons were scattered throughout the medial raphe (MR) and suprallemniscal cell group (B9). Stereological cell counting showed that approximately 36% of 5HT neurons in the RN nuclei co-expressed VGLUT3 in control animals (8003  $\pm$  925 5HT+/VGLUT3+ neurons, among 22,504  $\pm$  513 5HT neurons,

$n = 3$ ). For conditional ablation of VGLUT3 in serotonergic neurons we used *Pet1<sup>Cre/+</sup>;VGLUT3<sup>fl/fl</sup>* (VGLUT3-cKO) animals. VGLUT3-cKO mice did not show evidence of reduced 5HT neuron number (22,336  $\pm$  1187 5HT neurons,  $n = 3$ ,  $p = 0.94$ ), but only ~5% of 5HT+ neurons expressed VGLUT3 (1109  $\pm$  211 neurons,  $n = 3$ ,  $p < 0.01$ ) (Fig. 1b). Examination of 5HT+ axons in the caudal VTA revealed that 53  $\pm$  0.7% of 5HT+ axon boutons are VGLUT3+ in control animals and 14  $\pm$  4.8% of 5HT+ axon boutons co-label for VGLUT3 in VGLUT3-cKO animals ( $n = 3$ ; 122  $\pm$  13 buttons per animal; Fig. 1c).

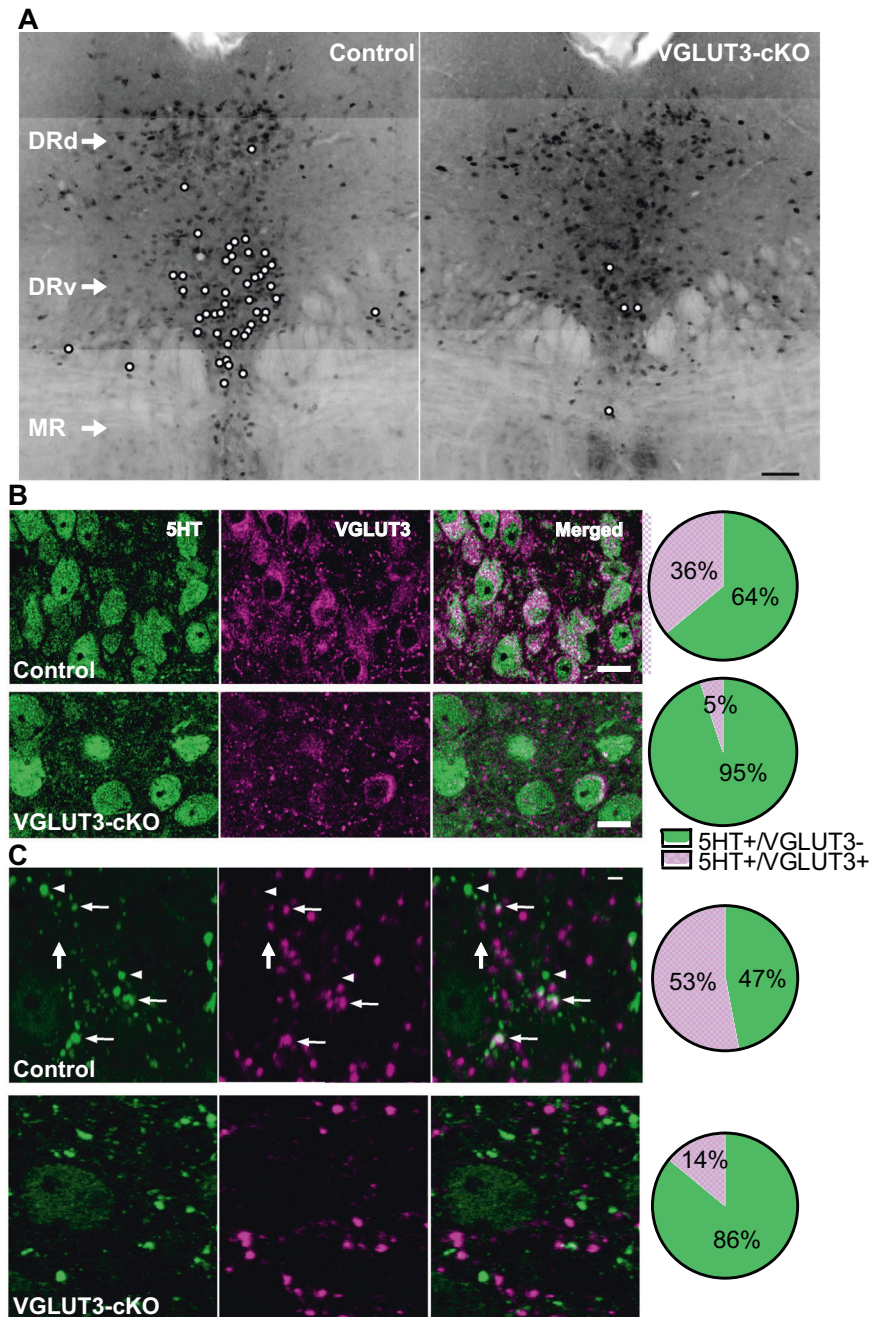
### Optogenetic activation of serotonergic terminals in the VTA activates DAergic neurons via glutamate

To see how serotonergic cell activity modulates cell circuit function and behavior, we established a mouse line that expresses a channelrhodopsin2-enhanced yellow fluorescent fusion protein (ChR2-eYFP) exclusively in serotonergic neurons [24]. We combined the *ai32* allele, which consists of floxed-STOP ChR2-eYFP cassette targeted to the (Gt) ROSA26Sor locus [20], with the transgenic *ePet1-Cre* allele, which expresses Cre-recombinase under the *pet1* promoter, exclusively active in serotonergic neurons [19]. To establish the specificity and efficiency of the *Pet1<sup>Cre/+</sup>* transgene, we evaluated the colocalization of eYFP and 5HT immunolabeling in *Pet1<sup>Cre/+</sup>;ChR2<sup>fl/fl</sup>* mice ( $n = 2$ ). We found that 95.1% of 5HT+ neurons clearly expressed ChR2-eYFP (23,656 ChR2-eYFP+/5HT+ in a total of 24,876 5HT+), and 82.7% of ChR2-eYFP+ neurons clearly expressed 5HT (23,656 ChR2-eYFP+/5HT+ in a total of 28,845 ChR2-eYFP+; Fig. 2a).

To characterize the functional connections of 5HT+ neurons to DAergic neurons, we performed whole-cell recordings of synaptic responses from DAergic neurons in the VTA and SN. To identify DAergic neurons, we injected a viral vector expressing dsRed fluorescent protein driven by the TH promoter (AAV-TH-dsRed) in the ventral mid-brain (Fig. 2b). Red fluorescent protein (RFP) was expressed mostly in the VTA and some in medial SN. Nearly all RFP+ (magenta) neurons were also TH+ (green), showing high specificity of RFP expression (Fig. 2c). We recorded firing of DAergic neurons in the mVTA, lateral VTA (lVTA) and SNc during 5HT terminal activation with train photostimulation (5 pulses at 20 Hz of blue light) (Fig. 2d–f). 5HT terminal stimulation elicited three types of responses: a firing increase, no effect, or firing pause (Fig. 2f). To evaluate change in firing, we calculated firing *z*-scores during train stimulation (0–0.3 s from onset of the train), compared with the preceding baseline. A positive *z*-score indicates a firing increase, while a negative *z*-score indicates a decrease. In 6 of 16 recorded mVTA DAergic neurons, firing increased during train stimulation, while only one cell

### Fig. 1 Serotonin—VGLUT3 colocalization.

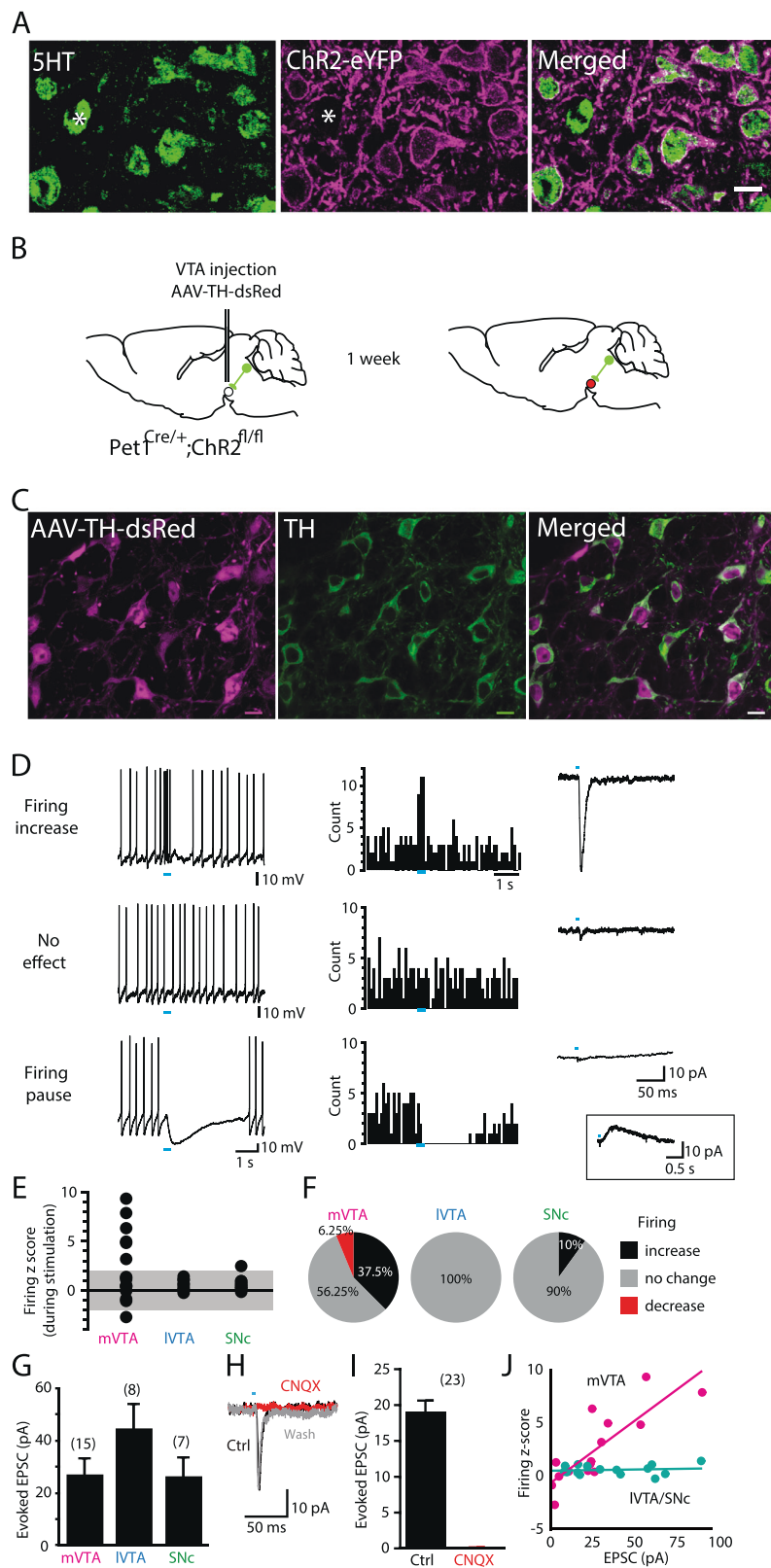
Immunofluorescence labeling was used to evaluate the number and distribution of VGLUT3+/5HT+ cells. **a** The distribution of VGLUT3+/5HT+ cells (white dots) was plotted onto low magnification photomontages of immunofluorescence-labeled 5HT cells. The photomontages were digitally inverted to enhance contrast. VGLUT3+/5HT+ cells were concentrated in the ventral subdivision of the dorsal raphe (DRv) with fewer cells in its dorsal subdivision (DRd) and lateral (DRl) divisions, and with scattered cells throughout the medial raphe (MR) and suprallemniscal (B9) cell group. In *Pet1<sup>Cre/+</sup>;VGLUT3<sup>fl/fl</sup>* (VGLUT3-cKO) animals only a few VGLUT3+/5HT+ were found. **b** High magnification images at the level of the DRv show 5HT cells with VGLUT3+ labeling that were common in control animals but sparse in VGLUT3-cKO animals. Stereological quantification found VGLUT3 expression in about 36% of 5HT cells in control animals, but only in 5% of 5HT cells in VGLUT3-cKO animals. **c** Counts of 5HT axon boutons in the caudal VTA found that about 47% were co-labeled with VGLUT3 in control animals (top) whereas 14% were co-labeled in VGLUT3-KO animals (bottom). Scale bar in **a** = 100  $\mu$ m, **b** = 10  $\mu$ m, **c** = 2  $\mu$ m.



showed a firing pause and the rest did not a change (Fig. 2e, f). In the IVTA and SNc, most DAergic neurons did not show significant changes; only one SNc DAergic neuron showed a modest increase in firing (Fig. 2e, f).

Under voltage clamp at  $-70$  mV, a single 0.1 Hz stimulation generated fast inward currents in DAergic neurons (Fig. 2d, right). In the sole neuron showing a firing pause in the mVTA, fast EPSCs were negligible, but slow outward currents were observed (Fig. 2d, bottom, right, inset). Average amplitude of EPSCs was  $27.0 \pm 6.2$  pA in the mVTA,  $44.6 \pm 9.5$  pA in the IVTA, and  $26.3 \pm 7.2$  in the

SNc, without significant regional differences (Fig. 2g; one-way ANOVA,  $F_{(2, 28)} = 1.63$ ,  $p = 0.21$ ). EPSCs in DAergic neurons were blocked by bath application of the AMPA receptor antagonist CNQX (40  $\mu$ M) (Fig. 2h, i; Paired  $t$  test:  $t_{(22)} = 12.13$   $df = 22$ ,  $p < 0.0001$ ). EPSC amplitude significantly correlated with firing  $z$ -score in the mVTA (linear regression;  $R^2 = 0.69$ ,  $p = 0.0001$ ; Fig. 2j), but not in the IVTA/SNc ( $R^2 = 0.017$ ,  $p = 0.64$ ). EPSC amplitudes did not show a regional difference, and only mVTA EPSCs positively correlated to DA neuron firing. This regional correlation in excitability was not due to differences in input



resistance or action potential threshold (one-way ANOVA;  $F_{(2,25)} = 0.49$ ,  $p = 0.62$ ;  $F_{(2,31)} = 0.09$ ,  $p = 0.92$ , respectively; Supplemental Fig. 1A, B). Rather the different time

course of the afterhyperpolarization during spontaneous firing ( $F_{(2,31)} = 13.5$ ,  $p < 0.001$ ), and not its amplitude ( $F_{(2,31)} = 2.7$ ,  $p = 0.08$ ), appeared to account for regional

**◀ Fig. 2 Optogenetic stimulation of serotonergic terminals activates dopaminergic cells via glutamate.** **a** Double immunofluorescence showed that in  $\text{Pet1}^{\text{Cre/+}};\text{ChR2}^{\text{fl/fl}}$  animals, ChR2-eYFP was highly co-expressed with 5HT throughout the raphe nucleus, although occasional cells expressed only 5HT (asterisk). **b** To label dopaminergic cells we injected AVV-TH-dsRed into the VTA of  $\text{Pet1}^{\text{Cre/+}};\text{ChR2}^{\text{fl/fl}}$  mice (left). A green cell and axon indicate 5HT neuron expressing ChR2-EYFP and its projection to the ventral midbrain. One week after injection, VTA-DAergic neurons expressed RFP (right, red cell). **c** RFP expression (magenta) and TH immunostaining (green) in the VTA from AAV-Th-dsRed injected  $\text{Pet1}^{\text{Cre/+}};\text{ChR2}^{\text{fl/fl}}$  mice. Scale bar = 10  $\mu\text{m}$ . **d** Sample traces from RFP+ cells in the medial VTA (mVTA). (Left) Sample traces of DAergic neuron firing, showing firing increase (top), no effects (middle), and firing pause (bottom) in response to a train stimulus onto 5HT neuron terminals. A train stimulus of 5 pulses at 20 Hz (470 nm, 5 ms duration) was applied at the time indicated by the blue bars. (Middle) Peristimulus histograms of action potentials made from 10 consecutive traces shown in left column. The bin width is 100 ms. The timing of a stimulation train is indicated by blue bars. (Right) Sample traces of fast EPSCs at  $-70$  mV, recorded from the same cells after firing. The EPSCs were evoked by a single stimulus at 0.1 Hz. Timings of the stimulation are shown with blue lines. In the cell that showed firing pause (bottom), slow outward currents were observed, whose entire time course is shown in the inset. **e** Distribution of firing Z-scores in the mVTA, lateral VTA (lVTA), and substantia nigra pars compacta (SNc). Gray shaded area shows 'no effect' range:  $<2$  SD change from baseline. **f** Pie chart showing ratio of firing responses in each region. Firing increase (black) indicates Z-score  $>2$  (more than 2 SD increase), firing decrease (red) indicates Z-score  $<-2$  (more than 2 SD decrease), and no effect (gray) indicates Z-score is between  $-2$  and  $2$ , in gray shaded area in (d). **g** Average peak amplitude of EPSCs evoked by a single 0.1 Hz stimulus in the three ventral midbrain regions. **h, i** The fast EPSCs were mediated by AMPA/kainite receptors. **h** Sample traces of the fast EPSCs evoked by a single stimulus at 0.1 Hz recorded from mVTA DA neurons under control condition (Ctrl, black), after application of  $40 \mu\text{M}$  CNQX (red), and after wash (gray). **i** Summary of the effects of CNQX. CNQX blocked the fast EPSCs ( $n = 23$ ,  $p < 0.001$ ). Sample EPSC traces were averages from 10 consecutive traces. Numbers of recorded cells are in parentheses. **j** Linear regression analysis of EPSC amplitudes and firing Z-scores. In the mVTA, EPSC amplitude and firing Z-scores were positively correlated (magenta,  $R^2 = 0.69$ ,  $p = 0.0001$ ), while no significant correlation was observed in merged lVTA/SNc (blue-green,  $R^2 = 0.017$ ,  $p = 0.64$ ).

differences (Supplemental Fig. 1C, D). The longer afterhyperpolarization kept the membrane potential more hyperpolarized and prevented glutamate EPSCs from reaching firing thresholds in lVTA/SNc DA neurons, in contrast to the shorter afterhyperpolarizations in mVTA DA neurons (Fig. 2d top; Supplemental Fig. 1E). These results show that 5HT neuron inputs can activate mVTA DA neurons via glutamatergic excitation.

### Optogenetic stimulation of RN serotonergic neurons or VTA serotonergic terminals results in hyperlocomotion and place-preference

Next, we studied the consequences of optogenetic stimulation of serotonergic neurons on locomotion and place preference. Stimulation of serotonergic neurons may cause

two opposing effects on VTA-DAergic neurons. 5HT release can inhibit DAergic tone via activation of 5HT<sub>2C</sub> receptors on VTA-GABAergic neurons [14]. Or, conversely, glutamate release from serotonin neuron terminals can directly activate DAergic neurons as observed in our electrophysiological experiments (Fig. 2). First, we tested  $\text{Pet1}^{\text{Cre/+}};\text{ChR2}^{\text{fl/fl}}$  ( $\text{Pet1-ChR2}$ ) mice and their non-ChR2-expressing littermate controls ( $\text{Pet1}^{\text{+/+}};\text{ChR2}^{\text{fl/fl}}$ ) in a real-time place preference protocol, with optical fiber implants in the DR (Supplemental Fig. 2A). Mice were placed in a two-compartment arena and allowed to explore both compartments freely; photostimulation (Light pulses: 473 nm, 20 Hz, 10 ms, 10 mW) was delivered whenever the mice were in the stimulated compartment. As seen in Supplemental Fig. 2B–E, mice started exploring both compartments equally, but as the experiment progressed,  $\text{Pet1-ChR2}$  mice spent increasingly more time in the stimulated compartment (repeated measures ANOVA; Time  $\times$  Location:  $F_{(5, 100)} = 6.556$ ,  $p < 0.0001$ ) while littermate controls showed no preference (repeated measures ANOVA; Time  $\times$  Location:  $F_{(5, 40)} = 1.652$ ,  $p = 0.1687$ ).

In a second cohort, we implanted optical fibers targeting the DR of  $\text{ePet1-ChR2}$  mice (Fig. 3a) and tested their locomotor response to optogenetic stimulation. Mice were placed in an open field and locomotion was recorded in 1.5 min bins. Optogenetic stimulation (Light pulses: 473 nm, 20 Hz, 10 ms, 10 mW), represented in the figures by blue vertical bars, resulted in an increase in distance traveled in  $\text{Pet1-ChR2}$  (Fig. 3b; Time  $\times$  Genotype:  $F_{(5, 135)} = 5.168$ ,  $p = 0.0002$ ). Next, we tested whether stimulating serotonergic neurons could induce conditioned-place-preference (in contrast to the real-time place preference from Supplemental Fig. 2). In the place-preference protocol, mice were free to explore a two-compartment arena for 20 min a day for 2 days. Each side of the box had distinct visual and tactile cues. One side of the chamber was paired with optical stimulation of the DR. On the third day, the mice were allowed to explore the box for 20 min without stimulation.  $\text{Pet1-ChR2}$  mice showed a strong preference for the previously stimulated side ( $t_{(19)} = 3.999$ ,  $p = 0.0008$ ) while their littermate controls spent approximately half their time in each chamber (Fig. 3c). Interestingly, the pattern of activity and conditioning place-preference seen in  $\text{Pet1-ChR2}$  animals was mimicked by optogenetic stimulation of DAergic neurons.  $\text{Dat}^{\text{IRES-Cre/+}};\text{ChR2}^{\text{fl/fl}}$  ( $\text{Dat-ChR2}$ ) animals implanted with optical fibers in the VTA (Fig. 3d) showed a similar increase in locomotion when submitted to the same protocol of photostimulation (Fig. 3e; Time  $\times$  Genotype:  $F_{(5, 60)} = 4.649$ ,  $p = 0.0012$ ). Similarly, photostimulation of DAergic neurons led to conditioned-place preference in  $\text{Dat-Cre}^{\text{+/+}};\text{Ai32}^{\text{+/+}}$  animals (Fig. 3f,  $t_{(11)} = 3.215$ ,  $p = 0.0082$ ).

To confirm the effects on locomotion were due to direct projections from the DR to the VTA, we examined effects



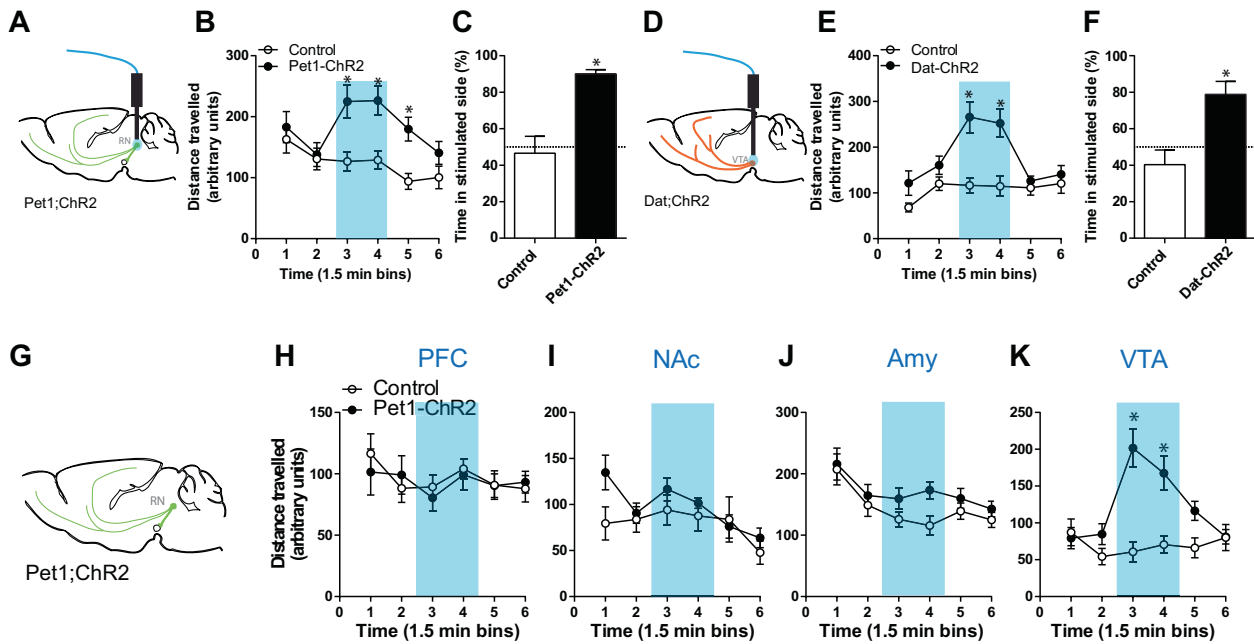


**Fig. 3 Optogenetic activation of serotonergic cells elicits place-preference and hyperlocomotion by activating the VTA.** **a, b** Pet1-ChR2 mice increased their locomotion in the open-field when receiving optical stimulation;  $n = 14-15$ . **c** Pet1-ChR2 mice and their littermate controls were subjected to a place-preference protocol. Mice were free to explore a 2-sided box for 20 min a day for 2 days. Each side of the box had distinct visual and tactile cues. One side of the chamber was paired with optical stimulation of the DR. On the third day, the mice were allowed to explore the box for 20 min without stimulation. Pet1-ChR2 showed a strong preference for the previously stimulated side while their littermate controls spent approximately half their time in each chamber;  $n = 9-11$ . **d, e** As with stimulation of

serotonergic cells expressing ChR2 in the DR, stimulation of ChR2-expressing dopaminergic cells in the VTA induced hyperlocomotion;  $n = 7-8$ . **f** Dat<sup>Cre/+</sup>:ChR2<sup>fl/fl</sup> (Dat-ChR2) and their littermate controls (Dat<sup>+/+</sup>:ChR2<sup>fl/fl</sup>) were subjected to the same place-protocol as in (c). Similarly, stimulation of dopaminergic cells induced conditioned-place-preference;  $n = 4-9$ . \* $p < 0.05$ . Vertical blue columns represent the periods of optical stimulation: 473 nm, 20 Hz, 10 ms, 10 mW. **(g-k)** Pet1-ChR2 mice, which express ChR2 in serotonergic terminals (Blue columns: 473 nm, 20 Hz, 10 ms, 10 mW) in the VTA (**k**) but not in the prefrontal cortex (PFC) (**h**), nucleus accumbens (NAC) (**i**), or amygdala (Amy) (**j**).  $n = 14-18$ ; \* $p < 0.05$ .

of 5HT neuron terminal stimulation in other projection regions. We found that only stimulation of serotonergic terminals in the VTA (Fig. 3g, k,  $F_{(5, 150)} = 7.150$ ,  $p < 0.0001$ ) but not in other regions (Fig. 3h-j) led to an increase in locomotion in Pet1-ChR2 animals. Consistently, optogenetic stimulation of serotonergic terminals in the VTA induced real-time place-preference (Supplemental Fig. 3, Time  $\times$  Location:  $F_{(3, 102)} = 19.92$ ,  $p < 0.0001$ ). Thus photostimulation of 5HT neurons increases VTA-DAergic neuron activity to increase locomotion.

### Postnatal-fluoxetine treatment results in deficits in glutamatergic transmission from serotonergic neurons to VTA-DAergic ones

Several studies have revealed that postnatal SSRI administration reduces exploration [4, 5]. Similarly, mice lacking 5HT transporters (SERT-KO mice) show striking reductions in exploration and activity in novelty-based tests [11]. This led us to hypothesize that an increase in serotonergic tone during development (caused by SERT inhibition) may result in DAergic dysfunction, and diminished behavioral

activation [41, 42]. To uncover the underlying mechanism of postnatal SSRI exposure related behavioral effects, we recorded serotonergic neuron glutamate EPSCs in VTA-DAergic neurons in brain slices made from control (saline treated) and postnatal fluoxetine-treated (Postnatal day 2-11; 10 mg/kg/day IP) Pet1-ChR2 mice (Fig. 4a).

First, we characterized the intrinsic electrophysiological properties of DAergic neurons in SSRI treated versus control mice, and observed no significant differences in resting electrical properties (Fig. 4b). We, therefore, conclude that early life fluoxetine exposure does not affect the electrical properties of these neurons. Next, we measured paired pulse ratios of glutamate EPSCs evoked by stimulating the 5HT input onto DAergic neurons in the mVTA with two blue light pulses at a 100 ms interval. We observed paired pulse depression (PPD) in all neurons; however PPD in neurons from fluoxetine-exposed mice was decreased, indicating a decrease in release probability at 5HT > DA neuron synapses (Fig. 4c, d,  $t_{(18)} = 3.095$ ,  $p = 0.0062$ ). Next, we compared AMPA/NMDA ratios in saline- and fluoxetine-treated mice. We performed whole-cell recordings from DAergic neurons in the mVTA while evoking AMPA

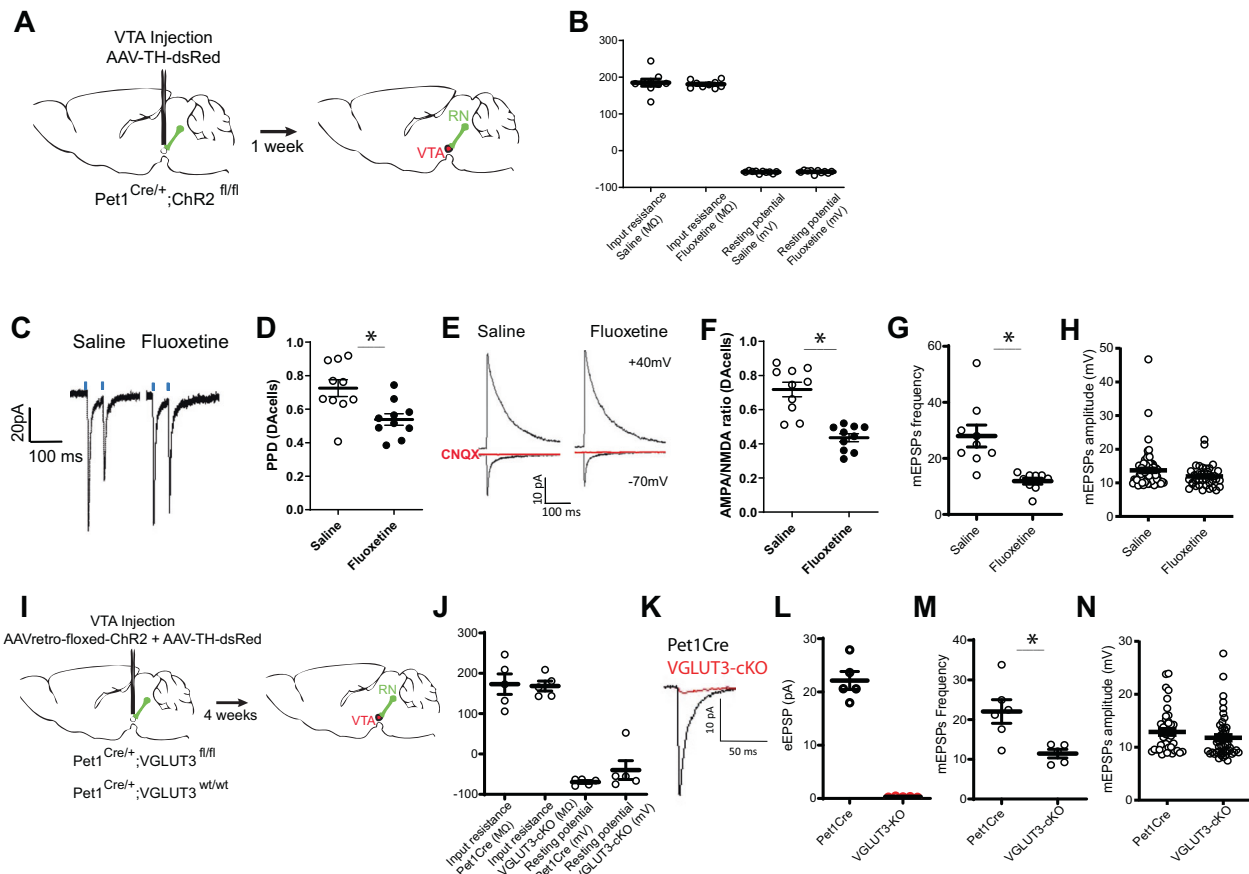


**Fig. 4** Postnatal-fluoxetine exposure led to deficits in glutamatergic transmission. **a** Experimental configuration and circuit schematic. Pet1-ChR2 mice were treated daily with fluoxetine (10 mg/kg) or saline from P2 to P11. After 3 months of age these mice were stereotactically infused with AAV-TH-dsRed into the VTA to label dopaminergic cells. One week later the brains were processed for electrophysiology. **b** Intrinsic electrophysiological properties of DAergic neurons of animals postnatally treated with saline or fluoxetine. **c** Sample traces of voltage clamp recording during paired pulse stimulation of the 5HT input onto DAergic neurons of the mVTA of saline injected versus fluoxetine-treated mice. **d** Summary graph of paired pulse ratios (PPR) evaluated at 100-ms intervals, whose values were calculated as the ratio of the second stimulus-evoked EPSC peak divided by the first stimulus-evoked EPSC peak. The PPRs of saline and fluoxetine injected mVTA slices (saline DAergic  $n = 10$ , fluoxetine DAergic  $n = 10$ ) were calculated from the averaged PPR values.

currents at  $-70$  mV, and NMDA currents at  $+40$  mV with photostimulations of 5HT neuron terminals. DAergic neurons from fluoxetine-exposed mice displayed a significant decrease in AMPA/NMDA ratios (Fig. 4e, f,  $t_{(18)} = 5.807$ ,  $p < 0.0001$ ). Interestingly, differences in paired pulse ratios and AMPA/NMDA ratios in postnatal fluoxetine-treated mice were observed in DAergic neurons but not VTA-GABAergic neurons (Supplemental Fig. 4). Changes in the probability of neurotransmitter release correlate with differences in paired-pulse ratio values [43, 44]. To test further our hypothesis that raphe-VTA glutamatergic synaptic transmission is affected by postnatal fluoxetine exposure we

examined miniature EPSPs, a measure of neurotransmitter release probability. Our data show that the frequency of mini-EPSPs is reduced in mice by early life fluoxetine exposure (Fig. 4g,  $t_{(16)} = 3.97$ ,  $p = 0.0011$ ). We did not observe differences in mini-EPSP amplitudes (Fig. 4h), arguing further for a presynaptic reduction in postnatal fluoxetine-exposed animals. To test whether the observed functional deficits were associated with structural deficits we quantified the total number of serotonergic cells in the raphe stereologically and their colocalization with VGLUT3. We did not find significant differences between postnatal treatments (Raphe

Pet1+ cells: Saline:  $29483 \pm 2205$ , Fluoxetine:  $31,739 \pm 1456$ ,  $n = 8-10$ ,  $t_{(16)} = 0.8838$ ,  $p = 0.39$ ; Raphe Pet1+/VGLUT3+: Saline  $8027 \pm 1357$ , Fluoxetine:  $8807 \pm 828$ ,  $n = 8-10$ ,  $t_{(16)} = 0.5121$ ,  $p = 0.62$ ). Nor did we find differences in the percent of Pet1 axons boutons that co-express VGLUT3 in the VTA (Saline:  $40.1\% \pm 5.5$ , Fluoxetine:  $46.8\% \pm 7.7$ ,  $n = 4$ ,  $t_{(6)} = 0.6419$ ,  $p = 0.54$ ), or in Pet1+ axonal density in the VTA evaluated as number of axon contacts per spherical probe (Saline:  $1.06 \pm 0.22$ , Fluoxetine:  $1.00 \pm 0.11$ ,  $n = 4$ ,  $t_{(6)} = 0.2474$ ,  $p = 0.81$ ).

To determine whether glutamatergic co-transmission is responsible for the observed neuronal activity modulation, we characterized the intrinsic electrophysiological properties of DAergic neurons in VGLUT3-cKO (Pet1<sup>Cre/+</sup>;VGLUT3<sup>fl/fl</sup>) versus control Pet1Cre mice (Pet1<sup>Cre/+</sup>;VGLUT3<sup>wt/wt</sup>) in whole-cell patch-clamp recordings (Fig. 4i, j). To express ChR2 in serotonergic projections to the VTA, we infused an AAVretro-EF1a-double floxed-hChR2 (Addgene #20298-AAVrg) in the VTA. At the same time, we infused a AAV-TH-dsRed virus to label DAergic neurons (Fig. 4i). No significant differences were observed between the resting electrical properties of Pet1Cre control and VGLUT3-cKO DAergic neurons (Fig. 4j). We next asked whether illumination of ChR2 would evoke EPSCs in DAergic neurons of VGLUT3-cKO and compared those to EPSCs of DAergic neurons in Pet1Cre mice. For this purpose, large spots ( $\approx 0.4 \text{ mm}^2$ ) of blue light were used to illuminate acute brain slices of the VTA. Illumination generated outward currents (Fig. 4k, l) in Pet1Cre mice. In stark contrast, EPSC amplitudes in DAergic neurons of VGLUT3-cKO mice were almost eliminated, confirming that the elicited currents were due to raphe neuron serotonin neuron glutamatergic co-transmission. Comparing miniature EPSPs in DAergic neurons in VGLUT3-cKO and Pet1Cre control mice showed that the frequency of mini-EPSPs in DAergic neurons was reduced in VGLUT3-cKO mice (Fig. 4m,  $t_{(9)} = 3.09$ ,  $p = 0.012$ ), while amplitude was unaffected (Fig. 4n), consistent with a decrease in the probability of neurotransmitter release. This pattern mimics that of fluoxetine-treated animals. These observations suggest that postnatal fluoxetine exposure weakens excitatory synaptic inputs from 5HT+ neurons to VTA-DAergic neurons by reducing the strength of the glutamate co-transmission. Furthermore, our data suggest that at least part of this deficit is mediated by diminished presynaptic neurotransmitter release.

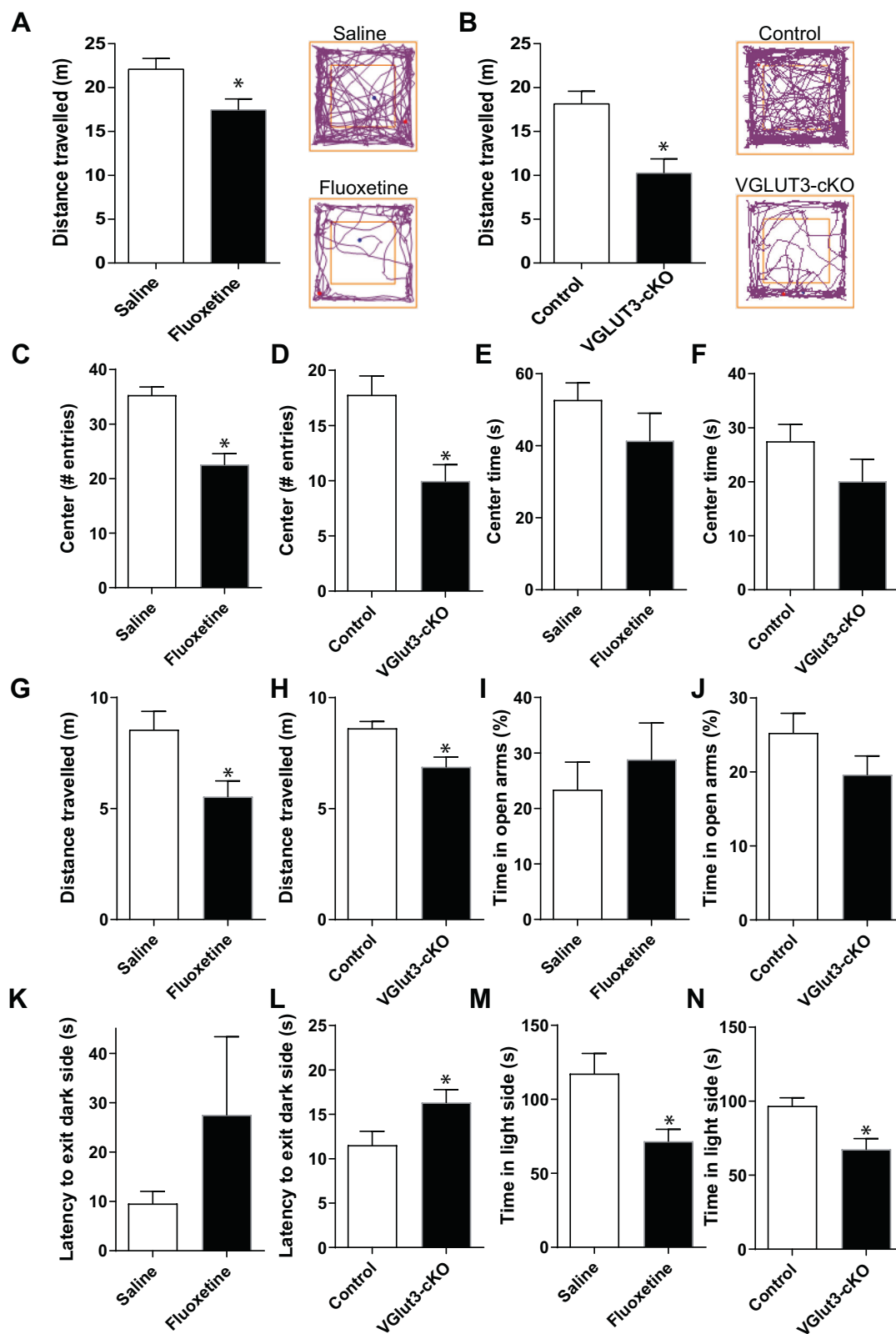
### Exploration deficits in postnatally fluoxetine-treated animals can be mimicked by VGLUT3 deletion and overridden by DAergic cell photostimulation

Previous studies have shown deficits in exploration in animals perinatally treated with SSRIs [4, 5]. Consistent with these results, we observed reduced locomotion in the open field in

animals treated with fluoxetine from P2 to P11 (Fig. 5a,  $t_{(29)} = 2.612$ ,  $p = 0.0141$ ). We hypothesized that this hypolocomotion was due to deficits in serotonergic neuron glutamate co-transmission to VTA-DAergic neurons. To test this hypothesis, we removed glutamate co-transmission from 5HT neurons by conditionally knocking out (VGLUT3-cKO) VGLUT3 from Pet1+neurons (Pet1<sup>Cre/+</sup>;VGLUT3<sup>fl/fl</sup>), and examined locomotion [22]. Interestingly, removing VGLUT3 from serotonergic neurons mimicked the hypolocomotion phenotype observed in mice administered fluoxetine during early life (Fig. 5b,  $t_{(22)} = 3.659$ ,  $p = 0.0014$ ).

To test whether other behavioral deficits induced by developmental exposure to SSRIs were similarly affected in VGLUT3-cKO mice we analyzed these two manipulations in the open-field, in the elevated-plus-maze and in Light-Dark choice. In addition to the deficits in distance traveled we observed a decrease in the number of center entries both in fluoxetine and VGLUT3-cKO mice (Fig. 5c, d). There was no difference in either group in the time spent in the center zone (Fig. 5e, f). On the elevated-plus maze, both fluoxetine-treated and VGLUT3-cKO mice showed a reduction in the total distance traveled in comparison to their respective controls (Fig. 5gh), but did not differ in the time spent in the open arms (Fig. 5i, j). In the light-dark choice test, only VGLUT3-cKO mice had an increased latency to exit the dark side (Fig. 5k, l). However, both fluoxetine-treated and VGLUT3-cKO mice spent significantly less time in the light side (Fig. 5m, n). The summary of the statistical results of these tests can be found in Supplemental Fig. 5. Together these data point to a strong influence of postnatal fluoxetine treatment on exploration that can be mimicked by the conditional deletion of VGLUT3 from 5HT+ neurons.

To test which behavioral phenotypes are affected by activation of the serotonergic system, mice were treated daily with fluoxetine (10 mg/kg) or saline from P2 to P11, and implanted with an optical fiber in the DR at 3 months of age. The mice were tested in the open-field, EPM, Forced-Swim-Test (FST), Novelty-Suppressed-Feeding (NST) or feeding in the home cage (Supplemental Fig. 6). As in the previous experiments, ChR2-negative mice that were exposed postnatally to fluoxetine showed a lower distance traveled in the open-field and EPM (Supplemental Fig. 6C, G). Also, they spent more time immobile in the FST (Supplemental Fig. 6K). Interestingly, although ChR2 activation during bouts of optogenetic stimulation increased locomotion in postnatal fluoxetine-treated mice, this activation was blunted when compared with that of saline-treated animals (Supplemental Fig. 6B, F). Consistent with our previous experiment, postnatal fluoxetine treatment did not alter time in the center in the open-field test (Supplemental Fig. 6E) nor time spent in the open arms in the EPM (Supplemental Fig. 6I). These two measures were not



affected by optogenetic stimulation (473 nm, 20 Hz, 10 ms, 10 mW). Interestingly, postnatal fluoxetine treatment increased the time for food deprived animals to explore and

eat a food pellet placed in the center of an open arena in the NSF test (Supplemental Fig. 6L). Optogenetic stimulation of the serotonergic system not only did not rescue this

**Fig. 5 Postnatal-fluoxetine exposure led to deficits in exploration that were mimicked by ablation of VGLUT3 in *Pet1*<sup>+</sup> cells.** **a** Mice were treated daily with fluoxetine (10 mg/kg) or saline from P2 to P11. After 3 months of age these mice were tested in the open-field. Postnatal-fluoxetine-treated mice showed significantly reduced locomotion in the open-field ( $n = 14-17$ ). Traces show locomotory path of a representative saline and fluoxetine-treated animal. **b** *Pet1*<sup>Cre/+</sup>;VGLUT3<sup>fl/fl</sup> mice (VGLUT3-cKO) showed significantly reduced locomotion in the open-field compared with controls (*Pet1*Cre<sup>-/-</sup>;VGLUT3<sup>fl/fl</sup>;  $n = 11-13$ ). Traces show locomotor path of a representative *Pet1*Cre-VGLUT3 and Control animal. **c, d** Number of center entries in the open-field in postnatal-fluoxetine treatment ( $n = 14-17$ ) or VGLUT3-cKO experimental groups ( $n = 11-13$ ). **e, f** Time in the center zone of the open-field in postnatal-fluoxetine treatment ( $n = 14-17$ ) or VGLUT3-cKO experimental groups ( $n = 11-13$ ). **g, h** Distance traveled in the elevated plus-maze in postnatal-fluoxetine treatment ( $n = 9-13$ ) or VGLUT3-cKO experimental groups ( $n = 25-26$ ). **i, j** Time in open arms in the elevated plus-maze in postnatal-fluoxetine treatment ( $n = 9-13$ ) or VGLUT3-cKO experimental groups ( $n = 25-26$ ). **k, l** Latency to exit the dark side on a light-dark test in postnatal-fluoxetine treatment ( $n = 9-13$ ) or VGLUT3-cKO experimental groups ( $n = 25-26$ ). **m, n** Time in the light side on a light-dark test in postnatal-fluoxetine treatment ( $n = 9-13$ ) or VGLUT3-cKO experimental groups ( $n = 25-26$ ). \* $p < 0.05$ .

phenotype but increased the time the mice took to eat the pellet. Notably, none of the Chr2 stimulated mice ate the food pellet until the end of the test (10 min) (Supplemental Fig. 6L). This phenotype was likely caused by the hyperlocomotor effects of stimulation, likely linked to activation of the DAergic system and consequent anorexia. To test whether this stimulation also reduced food intake in the home cage, we introduced a food pellet in the home cage of food deprived mice. We observed a significant reduction of food intake in Chr2-positive mice. Interestingly, this reduction of food intake was higher in saline-treated animals than in postnatal fluoxetine-treated mice (Supplemental Fig. 6M), further supporting the hypothesis of a blunted activation of this pathway.

Supporting our hypothesis that locomotion deficits in fluoxetine-treated animals are due to deficits downstream of the RN, likely in the RN > VTA connection, photoactivation of serotonergic cell bodies in the RN (Supplemental Fig. 7,  $F_{(23, 230)} = 3.807$ ,  $p < 0.0001$ ) or serotonergic terminals in the VTA, using *Pet1*<sup>Cre/+</sup>;Chr2<sup>fl/fl</sup>, did not fully rescue the hypolocomotor phenotype (Fig. 6a, b, SSRI treatment:  $F_{(1, 14)} = 15.99$ ,  $p = 0.0013$ ). However, photostimulation of DA neurons in the VTA, downstream of the RN, in *Dat*<sup>ires-Cre/+</sup>;Chr2<sup>fl/fl</sup> mice, completely abolished the phenotype (Fig. 6c, d, SSRI treatment:  $F_{(1, 8)} = 0.08498$ ,  $p = 0.7781$ ). Supplemental Fig. 8 shows the lack of effect of photostimulation on Control, Chr2-negative animals and a reduction in postnatal fluoxetine-treated animals (SSRI treatment:  $F_{(1, 15)} = 5.877$ ,  $p = 0.0284$ ), suggesting that the increase in locomotion was not an artifact of blue light illumination. Supplemental Fig. 9 shows the placement of the fibers in the experiments performed.

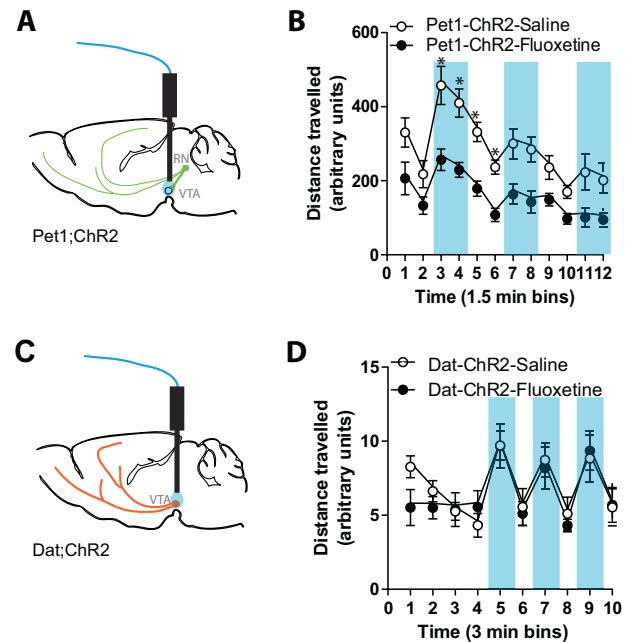


**Fig. 6 Stimulation of serotonergic terminals in the VTA did not fully rescue the hypolocomotor phenotype of fluoxetine-treated mice. Stimulation of dopaminergic cells did.** Mice were treated daily with fluoxetine (10 mg/kg) or saline from P2 to P11. After 3 months of age these mice were subjected to stereotaxic surgery and then tested in the open-field. **a** *Pet1*-Chr2 mice were implanted with optical fibers targeting the VTA;  $n = 8-9$ . **b** *Pet1*-Chr2 mice were placed in an open-field and their locomotion was recorded in 1.5 min bins. We observed lower locomotion in fluoxetine-treated animals even during optogenetic stimulation periods (vertical blue bars: 473 nm, 20 Hz, 10 ms, 10 mW). **c** *Dat*-Chr2 mice were implanted with optical fibers targeting the VTA. **d** *Dat*-Chr2 mice were placed in an open-field and their locomotion was recorded in 3 min bins. We observed no difference between saline and fluoxetine-treated animals;  $n = 5$ ; \* $p < 0.05$ .

## Discussion

Our results show that modulation of the levels of 5HT during development has life-long effects on glutamatergic function of serotonergic neurons. Our data confirmed that serotonergic neuron inputs to the VTA express the glutamatergic marker VGLUT3. Also, we showed that photostimulation of serotonergic terminals in the VTA can excite DAergic neurons through AMPA receptors. Photostimulation of these serotonergic terminals in the VTA led to increased locomotion and promoted place preference. Blocking SERT during development using the SSRI fluoxetine led to reduction in glutamatergic co-transmission between serotonergic and DAergic neurons and decreased exploratory activity. The decrease of exploration was mimicked by removal of glutamate co-transmission in serotonergic neurons. The decrease of locomotion in fluoxetine-treated animals was not fully rescued by stimulation of serotonergic cell bodies or serotonergic terminals

in the VTA but was fully abolished by stimulation of downstream VTA-DAergic neurons

### Serotonergic—DAergic interaction

Classical studies suggest opposite roles of 5HT and DA, with inhibitory effects of 5HT on DAergic activity [12–14, 45–48]. 5HT inhibits the reinforcement effects of intracranial self-stimulation [12, 49–51] and the serotonergic system is activated by noxious stimuli [52]. Chronic blockade of SERT elicits dysfunction in the basal ganglia that manifests as motor impairments that can be reversed by administration of L-DOPA [53]. Several side effects of SSRIs are thought to be DA-dependent and linked to DAergic inhibition: extrapyramidal symptoms, sexual dysfunction, cognitive dysfunction [reviewed in [54]]. Interestingly, accumbens DA is implicated in effort-related processes [41, 55] and although SSRIs are used to treat depression, they do not improve or have a negative impact on motivated behaviors [56]. Moreover, 5HT is thought to control aggression by an inhibitory control of DAergic activity [57].

Serotonergic neurons have been shown to have the ability to signal via glutamate as well as 5HT [21, 58]. VGLUT3 was found to be the VGLUT present in serotonergic neurons [21, 58]. Few studies have addressed the role of glutamatergic neurons in the RN. Consistent with our results, Luo's group first found that photostimulation of serotonergic neurons leads to place-preference, self-stimulation and activation of DAergic neurons via glutamatergic co-transmission [15]. However, two other groups did not find that activation of serotonergic neurons led to place-preference [17, 18]. At around the same time, Morales' group described a glutamatergic reward input from RN to VTA [59]. Together this led to the hypothesis that while serotonergic cells mediated patience, the DR to VTA pathway mediating reward was non-serotonergic [60]. However, recently, the Morales group extensively described the DR to VTA connection mediating reward as co-transmitting both serotonin and glutamate [16]. Furthermore, this study showed that stimulation of serotonergic terminals in the VTA evoked DA release in the NAc [16]. Consistent with the results from the Luo and Morales groups we show that DAergic neurons can be activated by serotonergic neurons via glutamate co-transmission. Importantly, we further show that early life manipulation of 5HT transmission can have an enduring effect on the strength of this co-transmission.

### Dopaminergic role in behavioral activation

DA is the key neurotransmitter involved in behavioral activation. Depletion or antagonism of DA in the NAc

suppresses novelty induced locomotion [61–64], and locomotor activity is reduced by inactivation of VTA DA neurons using DREADDs (designer receptors exclusively activated by designer drugs) [65]. Consistently, DA mediates behavioral activation and energy expenditure [66–69]. Here, we showed that activation of DAergic neurons in the VTA leads to increased locomotion and development of place-preference, suggesting that this activation is rewarding. Similarly, we observed that stimulation of serotonergic neurons in the raphe or serotonergic terminals in the VTA led to the same phenotype. Together with our electrophysiological results, these data support the hypothesis that activation of serotonergic terminals in the VTA excites DAergic neurons leading to behavioral activation.

Recorded mVTA DA neurons were located close to the midline, corresponding to the interfascicular nucleus or ventral part of the caudal linear nucleus. Those neurons project to the NAc medial shell [70–72]. IVTA neurons were recorded from the lateral part of the parabrachial pigmented nucleus, and DA neurons in this area project to the NAc lateral shell [72–74]. Therefore, serotonergic neuron inputs to the mVTA are likely to cause preferential activation of DA neurons projecting to the NAc medial shell. Activation of DA neuron terminals in the NAc medial shell conveys salience [75]; e.g., DA release is increased by consuming food or entering a new environment [76, 77]. Although interference with the NAc core function disrupts normal locomotion [78], injection of a psychostimulant into the NAc medial shell has been shown to increase locomotion [79, 80], and optical stimulation of ventral hippocampal inputs to the medial shell enhances cocaine-induced hyperlocomotion [81]. These observations suggest that the NAc shell, and not only the core, is involved in modulating locomotion.

### Increased 5HT levels during development and behavioral inhibition

Although most antidepressants work by blocking SERT, paradoxically, SERT-KO mice show behavioral traits opposite to those of mice exposed to antidepressants [4]. This was found to be due to blockage of SERT during development. SERT-KO mice as well as mice and rats exposed to SSRIs postnatally show an anxiety-like phenotype, with reduced exploration and reduced social interaction [4, 5, 25, 82–84], behavioral deficits that can arise from deficits in behavioral activation. P2 to P11 appears to identify a critical period, as SSRI treatment during this time window leads to behavioral deficits that are not observed if treatment is initiated later [5, 25]. Both SERT-KO mice and mice exposed to fluoxetine from P2 to P11 have reduced activity in the open-field [5, 11]. Consistent with these results, we similarly found that fluoxetine exposure from P2

to P11 leads to hypolocomotion in the open field. Given the role of DA in behavioral activation, these observations point to a hypodopaminergic state in these mice. Indeed, optogenetic stimulation of DAergic neurons abolished this phenotype, suggesting a deficit downstream of the serotonergic system but not downstream of the DAergic system. Importantly, we showed that glutamatergic transmission from serotonergic to DAergic neurons was reduced in fluoxetine-treated mice. Increased serotonergic tone during development may have led to an inhibition of the development of the serotonergic system via a negative-feedback mechanism.

Postnatal-fluoxetine treatment reduced strength of serotonergic neuron glutamate co-transmission presynaptically by reducing release probability and postsynaptically by reducing AMPA receptor insertion at the synaptic site. These results show a marked permanent set-point change in the DR > VTA pathway due to in vivo exposure to fluoxetine during postnatal life.

These results highlight a marked form of long-term synaptic plasticity modulation of the DR > VTA pathway elicited by early life exposure to fluoxetine, which may reflect a permanent and marked change in the network's set-point. High-levels of serotonin during development can produce negative feedback leading to a blunted serotonergic development via serotonin autoreceptors [85, 86]. Another underlying mechanism for this prolonged effect could be the modulation of epigenetic factors [87, 88] that regulate normal development and cell differentiation [89], and also play a role in neuroplasticity [90–93]. For example, it has been shown that MeCP2 and the MBD1 are significantly induced after repeated injections of fluoxetine for 10 days [94]. Furthermore, serotonin was recently shown to have a direct role in controlling gene expression via serotonylation of Histone 3 [95].

The relevance of these observations for humans is based on the high prevalence of risk factors for increased 5HT levels during development, e.g., maternal inflammation [86] and the substantial use of SSRIs (~10%) by women during pregnancy [96, 97]. Recent studies have implicated gestational exposure to SSRIs in the development of psychiatric disorders. In a Finish national registry study, by age 14.9 years the incidence of depression in 15,729 offspring exposed prenatally to SSRIs was 8.2% compared with 1.9% in the 9651 offspring of mothers with psychiatric disorders that had not been received SSRIs [7].

Our work demonstrates a role of serotonergic neurons in reward involving glutamate co-transmission of serotonergic neurons synapsing onto VTA-DAergic neurons. We furthermore find the strength of this connection to be set during a developmental period that is sensitive to serotonin signaling; serotonin-transporter blockade during P2-11 robustly weakens the capacity of serotonergic neurons to

excite VTA-DAergic neurons in adulthood leading to reduced exploratory activity of novel environments. Such novelty induced behavioral inhibition is one of the behavioral phenotypes which mice display after developmental SSRI exposure which relates to the depression-like phenotype seen in a recent epidemiological study [7]. Together our data provide translational insight into developmental mechanisms underlying endophenotypes of neuropsychiatric disorders. Such insights into how environmental factors can confer risk for later-occurring disorders could be relevant to efforts to improve prevention, advance age of first diagnoses and enhance treatment outcomes.

**Acknowledgements** This work has been supported by the National Institute of Child Health and Human Development (R01 HD095966 and R03 HD094978, CMT) and the National Institute on Drug Abuse (R01 DA038966, SR).

**Author contributions** CMT and MSA designed the experiments. CMT, CC, JFS, NC, CB, ECM and RS performed the experiments and analyzed the data. RPS, RHE and SR contributed new reagents or analytic tools. CMT, CC, JFS, NC, MSA and FXC wrote the paper with contributions from all co-authors.

## Compliance with ethical standards

**Conflict of interest** The authors declare that they have no conflict of interest.

**Publisher's note** Springer Nature remains neutral with regard to jurisdictional claims in published maps and institutional affiliations.

## References

- Deneris E, Gaspar P. Serotonin neuron development: shaping molecular and structural identities. *Wiley Interdisci Rev Dev Biol*. 2018;7:e301. <https://doi.org/10.1002/wdev.301>.
- Sodhi MS, Sanders-Bush E. Serotonin and brain development. *Int Rev Neurobiol*. 2004;59:111–74.
- Shah R, Courtiol E, Castellanos FX, Teixeira CM. Abnormal serotonin levels during perinatal development lead to behavioral deficits in adulthood. *Front Behav Neurosci*. 2018;12:114.
- Ansorge MS, Zhou M, Lira A, Hen R, Gingrich JA. Early-life blockade of the 5-HT transporter alters emotional behavior in adult mice. *Science*. 2004;306:879–81.
- Rebello TJ, Yu Q, Goodfellow NM, Caffrey Cagliostro MK, Teissier A, Morelli E, et al. Postnatal day 2 to 11 constitutes a 5-HT-sensitive period impacting adult mPFC function. *J Neurosci*. 2014;34:12379–93.
- Boukhris T, Sheehy O, Mottron L, Berard A. Antidepressant use during pregnancy and the risk of autism spectrum disorder in children. *JAMA Pediatr*. 2016;170:117–24.
- Malm H, Brown AS, Gissler M, Gyllenberg D, Hinkka-Yli-Salomaki S, McKeague IW, et al. Gestational exposure to selective serotonin reuptake inhibitors and offspring psychiatric disorders: a national register-based study. *J Am Acad Child Adolesc Psychiatry*. 2016;55:359–66.
- Beier KT, Steinberg EE, DeLoach KE, Xie S, Miyamichi K, Schwarz L, et al. Circuit architecture of VTA dopamine neurons revealed by systematic input-output mapping. *Cell*. 2015;162:622–34.

9. Russo SJ, Nestler EJ. The brain reward circuitry in mood disorders. *Nat Rev Neurosci.* 2013;14:609–25.
10. Salamone JD, Pardo M, Yohn SE, Lopez-Cruz L, SanMiguel N, Correa M. Mesolimbic dopamine and the regulation of motivated behavior. *Curr Top Behav Neurosci.* 2016;27:231–57.
11. Kalueff AV, Fox MA, Gallagher PS, Murphy DL. Hypolocomotion, anxiety and serotonin syndrome-like behavior contribute to the complex phenotype of serotonin transporter knockout mice. *Genes Brain Behav.* 2007;6:389–400.
12. Amit Z, Smith BR, Gill K. Serotonin uptake inhibitors: effects on motivated consummatory behaviors. *J Clin Psychiatry.* 1991;52 (Suppl):55–60.
13. Daw ND, Kakade S, Dayan P. Opponent interactions between serotonin and dopamine. *Neural Netw.* 2002;15:603–16.
14. Demireva EY, Suri D, Morelli E, Mahadevia D, Chuhma N, Teixeira CM et al. 5-HT<sub>2C</sub> receptor blockade reverses SSRI-associated basal ganglia dysfunction and potentiates therapeutic efficacy. *Molecular Psychiatry.* 2018.
15. Liu Z, Zhou J, Li Y, Hu F, Lu Y, Ma M, et al. Dorsal raphe neurons signal reward through 5-HT and glutamate. *Neuron.* 2014;81:1360–74.
16. Wang H-L, Zhang S, Qi J, Wang H, Cachepe R, Mejjas-Aponte CA, et al. Dorsal raphe dual serotonin-glutamate neurons drive reward by establishing excitatory synapses on VTA mesoaccumbens dopamine neurons. *Cell Rep.* 2019;26:1128–1142.e1127.
17. Fonseca MS, Murakami M, Mainen ZF. Activation of dorsal raphe serotonergic neurons promotes waiting but is not reinforcing. *Curr Biol.* 2015;25:306–15.
18. McDevitt RA, Tiran-Cappello A, Shen H, Balderas I, Britt JP, Marino RAM, et al. Serotonergic versus nonserotonergic dorsal raphe projection neurons: differential participation in reward circuitry. *Cell Rep.* 2014;8:1857–69.
19. Scott MM, Wylie CJ, Lerch JK, Murphy R, Lobur K, Herlitze S, et al. A genetic approach to access serotonin neurons for in vivo and in vitro studies. *Proc Natl Acad Sci USA.* 2005;102:16472–7.
20. Madisen L, Mao T, Koch H, Zhuo JM, Berenyi A, Fujisawa S, et al. A toolbox of cre-dependent optogenetic transgenic mice for light-induced activation and silencing. *Nat Neurosci.* 2012;15:793–802.
21. Gras C, Herzog E, Belenchi GC, Bernard V, Ravassard P, Pohl M, et al. A third vesicular glutamate transporter expressed by cholinergic and serotonergic neurons. *J Neurosci.* 2002;22:5442–51.
22. Divito CB, Steece-Collier K, Case DT, Williams S-PG, Stancati JA, Zhi L, et al. Loss of VGLUT3 produces circadian-dependent hyperdopaminergia and ameliorates motor dysfunction and l-Dopa-mediated dyskinesias in a model of Parkinson's Disease. *J Neurosci.* 2015;35:14983–99.
23. Backman CM, Malik N, Zhang Y, Shan L, Grinberg A, Hoffer BJ, et al. Characterization of a mouse strain expressing Cre recombinase from the 3' untranslated region of the dopamine transporter locus. *Genesis.* 2006;44:383–90.
24. Teixeira CM, Rosen ZB, Suri D, Sun Q, Hersh M, Sargin D, et al. Hippocampal 5-HT input regulates memory formation and schaffer collateral excitation. *Neuron.* 2018;98:992–1004.
25. Yu Q, Teixeira CM, Mahadevia D, Huang Y, Balsam DJ, Mann JJ, et al. Dopamine and serotonin signaling during two sensitive developmental periods differentially impact adult aggressive and affective behaviors in mice. *Mol Psychiatry.* 2014;19:688–98.
26. Smiley JF, Bleiwas C, Masiello K, Petkova E, Betz J, Hui M, et al. Effects of neonatal ethanol on cerebral cortex development through adolescence. *Brain Struct Funct.* 2019;224:1871–84.
27. West MJ, Slomianka L, Gundersen HJ. Unbiased stereological estimation of the total number of neurons in the subdivisions of the rat hippocampus using the optical fractionator. *Anat Rec.* 1991;231:482–97.
28. Commons KG. Ascending serotonin neuron diversity under two umbrellas. *Brain Struct Funct.* 2016;221:3347–60.
29. Muzerelle A, Scotto-Lomassese S, Bernard JF, Soiza-Reilly M, Gaspar P. Conditional anterograde tracing reveals distinct targeting of individual serotonin cell groups (B5-B9) to the forebrain and brainstem. *Brain Struct Funct.* 2016;221:535–61.
30. Dorph-Petersen KA, Nyengaard JR, Gundersen HJ. Tissue shrinkage and unbiased stereological estimation of particle number and size. *J Microsc.* 2001;204(Pt 3):232–46.
31. Mouton PR, Gokhale AM, Ward NL, West MJ. Stereological length estimation using spherical probes. *J Microsc.* 2002;206 (Pt 1):54–64.
32. Yizhar O, Fenno LE, Davidson TJ, Mogri M, Deisseroth K. Optogenetics in neural systems. *Neuron.* 2011;71:9–34.
33. Teixeira CM, Pomedli SR, Maei HR, Kee N, Frankland PW. Involvement of the anterior cingulate cortex in the expression of remote spatial memory. *J Neurosci.* 2006;26:7555–64.
34. Oh MS, Hong SJ, Huh Y, Kim KS. Expression of transgenes in midbrain dopamine neurons using the tyrosine hydroxylase promoter. *Gene Ther.* 2009;16:437–40.
35. Jia Y, Gall CM, Lynch G. Presynaptic BDNF promotes postsynaptic long-term potentiation in the dorsal striatum. *J Neurosci.* 2010;30:14440–5.
36. Kreitzer AC, Malenka RC. Endocannabinoid-mediated rescue of striatal LTD and motor deficits in Parkinson's disease models. *Nature.* 2007;445:643–7.
37. Teissier A, Chemiakine A, Inbar B, Bagchi S, Ray Russell S, Palmiter Richard D, et al. Activity of Raphe serotonergic neurons controls emotional behaviors. *Cell Rep.* 2015;13:1965–76.
38. Teixeira CM, Martin ED, Sahun I, Masachs N, Pujadas L, Corvelo A, et al. Overexpression of Reelin prevents the manifestation of behavioral phenotypes related to schizophrenia and bipolar disorder. *Neuropsychopharmacology.* 2011;36:2395–405.
39. Gaspar P, Lillesaar C. Probing the diversity of serotonin neurons. *Philos Trans R Soc Lond B Biol Sci.* 2012;367:2382–94.
40. Schäfer MK-H, Varoqui H, Defamie N, Weihe E, Erickson JD. Molecular cloning and functional identification of mouse vesicular glutamate transporter 3 and its expression in subsets of novel excitatory neurons. *J Biol Chem.* 2002;277:50734–48.
41. Salamone JD, Pardo M, Yohn SE, Lopez-Cruz L, SanMiguel N, Correa M. Mesolimbic dopamine and the regulation of motivated behavior. *Curr Topics Behav Neurosci.* 2016;27:231–57.
42. Yohn SE, Santerre JL, Nunes EJ, Kozak R, Podurgiel SJ, Correa M, et al. The role of dopamine D1 receptor transmission in effort-related choice behavior: Effects of D1 agonists. *Pharmacol Biochem Behav.* 2015;135:217–26.
43. Zucker RS. Short-term synaptic plasticity. *Annu Rev Neurosci.* 1989;12:13–31.
44. Ohana O, Sakmann B. Transmitter release modulation in nerve terminals of rat neocortical pyramidal cells by intracellular calcium buffers. *J Physiol.* 1998;513(Pt 1):135–48.
45. Juorio AV, Greenshaw AJ. The effect of raphe nuclei lesions on striatal tyramine concentration and dopamine turnover in the rat. *Neurochem Res.* 1986;11:687–93.
46. Williams J, Davies JA. The involvement of 5-hydroxytryptamine in the release of dendritic dopamine from slices of rat substantia nigra. *J Pharm Pharmacol.* 1983;35:734–7.
47. Nedergaard S, Bolam JP, Greenfield SA. Facilitation of a dendritic calcium conductance by 5-hydroxytryptamine in the substantia nigra. *Nature.* 1988;333:174–7.
48. Ugedo L, Grenhoff J, Svensson TH. Ritanserin, a 5-HT<sub>2</sub> receptor antagonist, activates midbrain dopamine neurons by blocking serotonergic inhibition. *Psychopharmacology.* 1989;98:45–50.
49. Abler B, Gron G, Hartmann A, Metzger C, Walter M. Modulation of frontostriatal interaction aligns with reduced primary reward processing under serotonergic drugs. *J Neurosci.* 2012;32:1329–35.



50. Di Matteo V, De Blasi A, Di Giulio C, Esposito E. Role of 5-HT (2C) receptors in the control of central dopamine function. *Trends Pharmacol Sci.* 2001;22:229–32.
51. Di Matteo V, Di Giovanni G, Pierucci M, Esposito E. Serotonin control of central dopaminergic function: focus on in vivo microdialysis studies. *Prog Brain Res.* 2008;172:7–44.
52. Schweimer JV, Ungless MA. Phasic responses in dorsal raphe serotonin neurons to noxious stimuli. *Neuroscience.* 2010;171:1209–15.
53. Morelli E, Moore H, Rebello TJ, Gray N, Steele K, Esposito E, et al. Chronic 5-HT transporter blockade reduces DA signaling to elicit basal ganglia dysfunction. *J Neurosci.* 2011;31:15742–50.
54. Damsa C, Bumb A, Bianchi-Demicheli F, Vidailhet P, Sterck R, Andreoli A, et al. “Dopamine-dependent” side effects of selective serotonin reuptake inhibitors: a clinical review. *J Clin Psychiatry.* 2004;65:1064–8.
55. Randall PA, Lee CA, Podurgiel SJ, Hart E, Yohn SE, Jones M, et al. Bupropion increases selection of high effort activity in rats tested on a progressive ratio/chow feeding choice procedure: implications for treatment of effort-related motivational symptoms. *Int J Neuropsychopharmacol.* 2015;18. pii: pyu017. <https://doi.org/10.1093/ijnp/pyu017>.
56. Yohn SE, Collins SL, Contreras-Mora HM, Errante EL, Rowland MA, Correa M, et al. Not all antidepressants are created equal: differential effects of monoamine uptake inhibitors on effort-related choice behavior. *Neuropsychopharmacology.* 2016;41:686–94.
57. Seo D, Patrick CJ, Kennealy PJ. Role of serotonin and dopamine system interactions in the neurobiology of impulsive aggression and its comorbidity with other clinical disorders. *Aggress Violent Behav.* 2008;13:383–95.
58. Amilhon B, Lepicard È, Renoir T, Mongeau R, Popa D, Poirel O, et al. VGLUT3 (Vesicular Glutamate Transporter Type 3) contribution to the regulation of serotonergic transmission and anxiety. *J Neurosci.* 2010;30:2198–210.
59. Qi J, Zhang S, Wang HL, Wang H, de Jesus Aceves Buendia J, Hoffman AF, et al. A glutamatergic reward input from the dorsal raphe to ventral tegmental area dopamine neurons. *Nat Commun.* 2014;5:5390.
60. McDannald MA. Serotonin: waiting but not rewarding. *Curr Biol.* 2015;25:R103–R104.
61. Koob GF, Riley SJ, Smith SC, Robbins TW. Effects of 6-hydroxydopamine lesions of the nucleus accumbens septi and olfactory tubercle on feeding, locomotor activity, and amphetamine anorexia in the rat. *J Comp Physiol Psychol.* 1978;92:917–27.
62. Cousins MS, Sokolowski JD, Salamone JD. Different effects of nucleus accumbens and ventrolateral striatal dopamine depletions on instrumental response selection in the rat. *Pharmacol Biochem Behav.* 1993;46:943–51.
63. Baldo BA, Sadeghian K, Basso AM, Kelley AE. Effects of selective dopamine D1 or D2 receptor blockade within nucleus accumbens subregions on ingestive behavior and associated motor activity. *Behav Brain Res.* 2002;137:165–77.
64. Correa M, Carlson BB, Wisniecki A, Salamone JD. Nucleus accumbens dopamine and work requirements on interval schedules. *Behav Brain Res.* 2002;137:179–87.
65. Marchant NJ, Whitaker LR, Bossert JM, Harvey BK, Hope BT, Kaganovsky K, et al. Behavioral and physiological effects of a novel Kappa-Opioid receptor-based DREADD in rats. *Neuropsychopharmacology.* 2016;41:402–9.
66. McCullough LD, Cousins MS, Salamone JD. The role of nucleus accumbens dopamine in responding on a continuous reinforcement operant schedule: a neurochemical and behavioral study. *Pharmacol Biochem Behav.* 1993;46:581–6.
67. Aberman JE, Ward SJ, Salamone JD. Effects of dopamine antagonists and accumbens dopamine depletions on time-constrained progressive-ratio performance. *Pharmacol Biochem Behav.* 1998;61:341–8.
68. Salamone JD, Wisniecki A, Carlson BB, Correa M. Nucleus accumbens dopamine depletions make animals highly sensitive to high fixed ratio requirements but do not impair primary food reinforcement. *Neuroscience.* 2001;105:863–70.
69. Ishiwari K, Weber SM, Mingote S, Correa M, Salamone JD. Accumbens dopamine and the regulation of effort in food-seeking behavior: modulation of work output by different ratio or force requirements. *Behavioural Brain Res.* 2004;151:83–91.
70. Kramer DJ, Risso D, Kosillo P, Ngai J, Bateup HS. Combinatorial expression of Grp and Neurod6 defines dopamine neuron populations with distinct projection patterns and disease vulnerability. *eNeuro.* 2018;5:ENEURO.0152-18.2018.
71. Baimel C, Lau BK, Qiao M, Borgland SL. Projection-target-defined effects of orexin and dynorphin on VTA dopamine neurons. *Cell Rep.* 2017;18:1346–55.
72. Ikemoto S. Dopamine reward circuitry: two projection systems from the ventral midbrain to the nucleus accumbens-olfactory tubercle complex. *Brain Res Rev.* 2007;56:27–78.
73. de Jong JW, Afjei SA, Pollak Dorocic I, Peck JR, Liu C, Kim CK, et al. A neural circuit mechanism for encoding aversive stimuli in the mesolimbic dopamine system. *Neuron.* 2019;101:133–151 e137.
74. Lammel S, Hetzel A, Hackel O, Jones I, Liss B, Roeper J. Unique properties of mesoprefrontal neurons within a dual mesocorticolimbic dopamine system. *Neuron.* 2008;57:760–73.
75. Mingote S, Amsellem A, Kempf A, Rayport S, Chuhma N. Dopamine-glutamate neuron projections to the nucleus accumbens medial shell and behavioral switching. *Neurochem Int.* 2019;129:104482.
76. Gambarana C, Masi F, Leggio B, Grappi S, Nanni G, Scheggi S, et al. Acquisition of a palatable-food-sustained appetitive behavior in satiated rats is dependent on the dopaminergic response to this food in limbic areas. *Neuroscience.* 2003;121:179–87.
77. Rebec GV, Grabner CP, Johnson M, Pierce RC, Bardo MT. Transient increases in catecholaminergic activity in medial prefrontal cortex and nucleus accumbens shell during novelty. *Neuroscience.* 1997;76:707–14.
78. Kelley AE. Functional specificity of ventral striatal compartments in appetitive behaviors. *Ann NY Acad Sci.* 1999;877:71–90.
79. Han X, Jing MY, Zhao TY, Wu N, Song R, Li J. Role of dopamine projections from ventral tegmental area to nucleus accumbens and medial prefrontal cortex in reinforcement behaviors assessed using optogenetic manipulation. *Metab Brain Dis.* 2017;32:1491–502.
80. Ikemoto S. Ventral striatal anatomy of locomotor activity induced by cocaine, D-amphetamine, dopamine and D1/D2 agonists. *Neuroscience.* 2002;113:939–55.
81. Britt JP, Benaliouad F, McDevitt RA, Stuber GD, Wise RA, Bonci A. Synaptic and behavioral profile of multiple glutamatergic inputs to the nucleus accumbens. *Neuron.* 2012;76:790–803.
82. Olivier JD, Valles A, van Heesch F, Afrasiab-Middelmann A, Roelofs JJ, Jonkers M, et al. Fluoxetine administration to pregnant rats increases anxiety-related behavior in the offspring. *Psychopharmacology.* 2011;217:419–32.
83. Olivier JDA, Åkerud H, Kaihola H, Pawluski JL, Skalkidou A, Högberg U, et al. The effects of maternal depression and maternal selective serotonin reuptake inhibitor exposure on offspring. *Front Cell Neurosci.* 2013;7:73.
84. Rincon-Cortes M, Barr GA, Mouly AM, Shionoya K, Nunez BS, Sullivan RM. Enduring good memories of infant trauma: rescue of adult neurobehavioral deficits via amygdala serotonin and corticosterone interaction. *Proc Natl Acad Sci USA.* 2015;112:881–6.
85. McDevitt RA, Neumaier JF. Regulation of dorsal raphe nucleus function by serotonin autoreceptors: a behavioral perspective. *J Chem Neuroanat.* 2011;41:234–46.

86. Goeden N, Velasquez J, Arnold KA, Chan Y, Lund BT, Anderson GM, et al. Maternal inflammation disrupts fetal neurodevelopment via increased placental output of serotonin to the fetal brain. *J Neurosci*. 2016;36:6041–9.
87. Avery OT, Macleod CM, McCarty M. Studies on the chemical nature of the substance inducing transformation of pneumococcal types: induction of transformation by a desoxyribonucleic acid fraction isolated from pneumococcus Type Iii. *J Exp Med*. 1944;79:137–58.
88. Hotchkiss RD. The quantitative separation of purines, pyrimidines, and nucleosides by paper chromatography. *J Biol Chem*. 1948;175:315–32.
89. Holliday R, Pugh JE. DNA modification mechanisms and gene activity during development. *Science*. 1975;187:226–32.
90. Jarome TJ, Perez GA, Hauser RM, Hatch KM, Lubin FD. EZH2 methyltransferase activity controls pten expression and mTOR signaling during fear memory reconsolidation. *J Neurosci*. 2018;38:7635–48.
91. Lubin FD, Gupta S, Parrish RR, Grissom NM, Davis RL. Epigenetic mechanisms: critical contributors to long-term memory formation. *Neuroscientist*. 2011;17:616–32.
92. Wang YJ, Okutani F, Murata Y, Taniguchi M, Namba T, Kaba H. Histone acetylation in the olfactory bulb of young rats facilitates aversive olfactory learning and synaptic plasticity. *Neuroscience*. 2013;232:21–31.
93. Miller CA, Sweatt JD. Covalent modification of DNA regulates memory formation. *Neuron*. 2007;53:857–69.
94. Cassel S, Carouge D, Gensburger C, Anglard P, Burgun C, Dietrich JB, et al. Fluoxetine and cocaine induce the epigenetic factors MeCP2 and MBD1 in adult rat brain. *Mol Pharm*. 2006;70:487–92.
95. Farrelly LA, Thompson RE, Zhao S, Lepack AE, Lyu Y, Bhanu NV, et al. Histone seronylation is a permissive modification that enhances TFIID binding to H3K4me3. *Nature*. 2019;567:535–9.
96. Huybrechts KF, Palmsten K, Mogun H, Kowal M, Avorn J, Setoguchi-Iwata S, et al. National trends in antidepressant medication treatment among publicly insured pregnant women. *Gen Hosp Psychiatry*. 2013;35:265–71.
97. Cooper WO, Willy ME, Pont SJ, Ray WA. Increasing use of antidepressants in pregnancy. *Am J Obstet Gynecol*. 2007;196:544 e541–545.